Chapter VII. Anomalous cross-field transport in edge plasma

VII.1 Introduction

As we discussed in Chapter VI, classical cross-field plasma transport is determined, roughly speaking, by two main components: charged particle motion in virtually stationary magnetic and electric fields and Coulomb collisions. Cross-field drift of charged particles related to inhomogeneity of the magnetic field, the direction of which depends on the sign of the charge, causes global polarization of the tokamak plasma column, accompanied by the $\vec{E}\times\vec{B}$ plasma convection, and, in addition, can result in a significant departure of the particles from their initial magnetic flux surfaces. On one hand, the Coulomb collisions control the electric current along the magnetic field lines, which balances plasma polarization due to the magnetic drift and, therefore, settles the intensity of the $\vec{E}\times\vec{B}$ plasma convection. On the other hand, the collisions "erase memory" of the charged particles on their "initial" magnetic flux surface and introduce a stochastic feature in the charged particle motion. As a result, even though the classical plasma energy and particle fluxes through magnetic flux surface are determined the by local plasma parameters and their gradients on the flux surface, the processes governing these fluxes (e.g. $\vec{E}\times\vec{B}$ plasma convection) happen on a "global" size-scale of the order of the tokamak minor radius a.

However, due to inhomogeneity of the density and temperature, the tokamak plasma, as we will see below, is often unstable. These instabilities result in the formation of electrostatic potential $\varphi(\vec{r},t)$ having filamentary structure extended along the magnetic field lines over some distance $\lambda_{||}$ and a relatively small characteristic cross-field size, $\lambda_{\perp} << a, \lambda_{||}$ (for simplicity we neglect perturbations of the magnetic field). Therefore, as an illustration, we consider the motion of a charged particle in a constant magnetic field $\vec{B}_0 = B_0\vec{e}_z$ and a 2D electrostatic potential, $\varphi(x,y,t)$, with a characteristic magnitude, φ_0, and a spatial scale length, $\lambda_{\perp}$, which varies on the time-scale $\tau_{\varphi} \sim \omega^{-1}$. Assume that $\lambda_{\perp}$ is larger than the particle gyro-radius whereas ω is smaller than the particle gyrofrequency. In this case, the charged particle will mostly experience $\vec{E}\times\vec{B}$ drift along the equipotentials of $\varphi(x,y,t)$ with a characteristic speed $V_{\vec{E}\times\vec{B}} \sim c\varphi_0/(\lambda_{\perp}B_0)$. However, the equipotentials can be considered "fixed" only for the time $t \lesssim \tau_{\varphi}$ and in this time, the particle would move to the distance $\delta \sim V_{\vec{E}\times\vec{B}}\tau_{\varphi}$ along the equipotentials, which we assume to be smaller than $\lambda_{\perp}$. If the "landscape" of the $\varphi(x,y,t)$ equipotentials is completely changed by the time $t \gtrsim \tau_{\varphi}$, then the particle at $t \gtrsim \tau_{\varphi}$ will drift along an equipotential completely different from what it was for $t \lesssim \tau_{\varphi}$. As a result, the distance δ can be considered as a "jump" of the particle on the (x,y) plane, which occurs in random directions within the time $\sim\tau_{\varphi}$ and particle transport in the $\varphi(x,y,t)$ potential has a diffusive nature. Taking into account that we assumed $\delta \lesssim \lambda_{\perp}$, and estimating $e\varphi_0 \sim T$ (where T is the

plasma temperature), we find that the particle diffusion coefficient $D_\varphi \lesssim D_B = cT/eB_0$, where D_B is the so-called Bohm diffusion coefficient.

This physical picture shows that the presence of electric field fluctuations having relatively small spatiotemporal scales can result in cross-field plasma transport exceeding, in practice, the classical one which is governed by quasi-stationary and large spatial scale processes.

However, in reality, anomalous cross-field plasma transport is much more complex. Nonlinear interactions of plasma fluctuations result, on the one hand, in some sort of self-regulation and even suppression of anomalous transport. On the other hand, they can change transport from relatively slow diffusive to very fast convective. Today we have no full understanding of all processes governing anomalous plasma transport. Therefore, in what follows, we present just very basic ingredients and features of anomalous plasma transport, with the emphasis on the processes more typical for the edge plasmas.

In this chapter, we adopt the following notations: all parameters with "tilde" are considered to be perturbations small in comparison with the stationary (or quasi-stationary) parameters having no "tilde" sign, or resulting in such small perturbations: e.g. a perturbation of the plasma density $\tilde{n}$ is much smaller than the background plasma density n ($|\tilde{n}|/n << 1$); $\tilde{\vec{V}}$ is a small perturbation of the velocity, which either is small in comparison with the background velocity $\vec{V}$, or produces a small variation of such plasma parameters as the pressure, density, etc.

VII.2 Linear theory of edge plasma instabilities

VII.2.1 Collisionless drift waves.

We start our consideration with the simplest physical picture of collisionless drift waves in plasma embedded into a constant magnetic field, $\vec{B} = B\vec{e}_z$ (where $\vec{e}_z$ is the unit vector in the z-direction). These waves are characterized by the frequency, ω, which is much lower than the ion gyrofrequency, Ω_{Bi}, so the charged particle motion across the magnetic field is largely described by the $\vec{E}\times\vec{B}$ drift. In addition, we consider such wave vectors, $\vec{k}$, that the phase velocity of the wave along the magnetic field lines, $\omega/k_{||}$, satisfies the following inequalities

$$V_{Ti} < \omega/k_{||} < V_{Te}, \qquad \text{(VII.1)}$$

where $k_{||} = \vec{k}\cdot\vec{B}/B$ is the wave vector component along the magnetic field, whereas $V_{Te} = \sqrt{T_e/m}$ and $V_{Ti} = \sqrt{T_i/M}$ are the electron and ion thermal velocities respectively. As a result, in this case, we largely can ignore the effects of the Landau resonances of the wave with both electrons and ions, which can play an important role in collisionless or weakly collisional plasmas.

First, we assume that the stationary plasma density, $n(x)$, is inhomogeneous in the x-direction, the electron temperature, T_e, is constant and an impact of the ion temperature can be neglected (the "cold" ion approximation). Let us now consider the evolution of a plasma slab, inclined at some small angle to the direction of the magnetic field, which is shifted in the x-direction from its original position (as shown in Fig. VII.1).

Since initially the plasma density was not homogeneous in the x-direction, such a protrusion will cause a weak plasma inhomogeneity along both z- and y-directions. As a result, the electrons, which are much lighter and, therefore, much faster than the ions, will try to escape from the plasma density bump, leaving the bulky and slow ions alone. However, this charge separation along the magnetic field can only go until the electric field that emerges from such plasma polarization stops further electron escape, see Fig.VII.1(a). We notice that due to the inclination of the shifted plasma slab, the resulting electric field has a component in the y-direction (see Fig.VII.1(b)), which will cause the $\vec{E}\times\vec{B}$ plasma drift in the x-direction. The direction of this $\vec{E}\times\vec{B}$ plasma drift will be different on the different slopes of the density protrusion: on one side it will move the plasma protrusion toward its initial position (and decrease the protrusion), whereas on the other one it will move the plasma out from its initial position (and increase the protrusion) as shown in Fig.VII.1(b). As a result, the plasma protrusion will be "advected" in the y-direction, exhibiting a wave-like motion. However, we note that even though such a wave of plasma density perturbation propagates in the y-direction, the displacement of the plasma density *per se* occurs only in the x-direction.

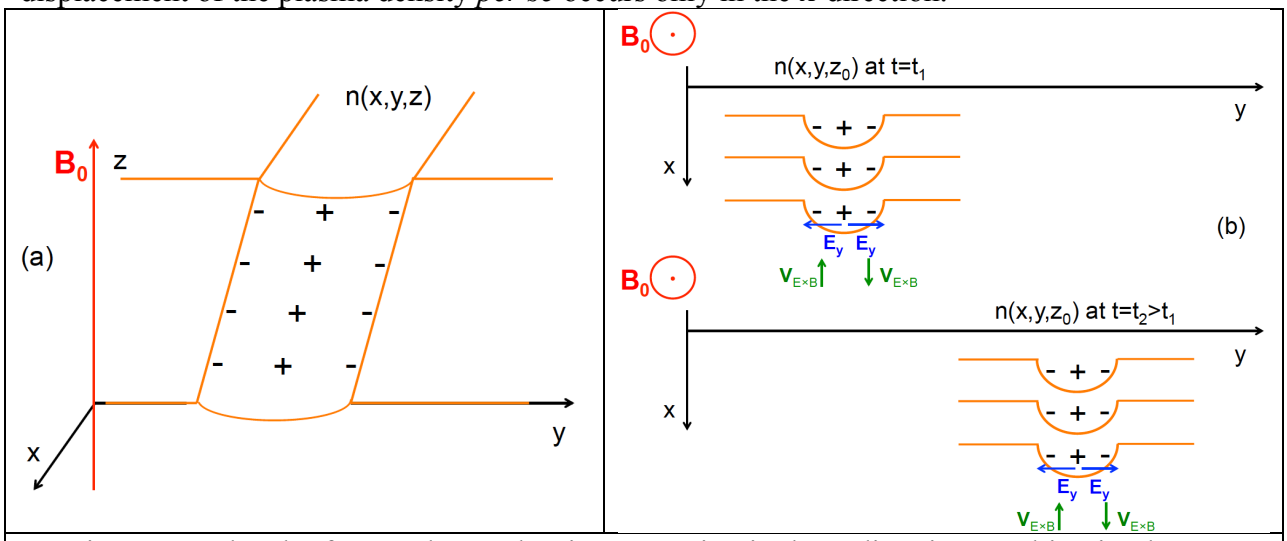

Fig. VII.1. Sketch of a 3D plasma density protrusion in the x-direction resulting in plasma polarization caused by the electron motion along the magnetic field lines (a); Advection of the plasma density contours at $z = z_0$ in the y-direction due to $\vec{E}\times\vec{B}$ drift in the x-direction (b).

This simplest physical picture of collisionless drift waves can be easily supplemented by a quantitative description (e.g. see [1], [2], [3], [4]). For this, we will assume that the perturbations of the plasma density, $\tilde{n}$, are small ($|\tilde{n}| << n$) and all nonlinear effects can be ignored. In addition, we will consider the characteristic wavelength of the perturbations much larger than the Debye length, and the plasma can be considered quasi-neutral, $\tilde{n}_e \cong \tilde{n}_i \equiv \tilde{n}$, even though some charge polarization effects exist. We will ignore the ion motion along the magnetic field lines and assume that parallel dynamics of fast electrons reaches equilibrium virtually instantaneously so the gradient of the electron pressure along the magnetic field is balanced by the electric force, which gives the Boltzmann relation for the perturbed electron density and electrostatic potential $\tilde{\varphi}$:

$$\frac{\tilde{n}_e}{n} = \frac{e\tilde{\varphi}}{T_e} \equiv \tilde{\phi}. \qquad \text{(VII.2)}$$

Finally, we assume that the cross-field plasma (both electron and ion) velocity is determined by $\vec{E}\times\vec{B}$ drift:

$$\vec{V}_{\vec{E}\times\vec{B}} = -\frac{c}{B^2}\left(\nabla\varphi\times\vec{B}\right). \qquad \text{(VII.3)}$$

Then, taking into account that for a straight constant magnetic field $\nabla\cdot\vec{V}_{\vec{E}\times\vec{B}} = 0$, we have the following form of the plasma continuity equation

$$\frac{\partial n}{\partial t} + \nabla\cdot\left(\vec{V}_{\vec{E}\times\vec{B}} n\right) \equiv \frac{\partial n}{\partial t} + \nabla n\cdot\vec{V}_{\vec{E}\times\vec{B}} = 0. \qquad \text{(VII.4)}$$

As a result, from expressions (VII.2, VII.4) we find

$$\frac{\partial\tilde{n}}{\partial t} + U_{dw}\frac{\partial\tilde{\phi}}{\partial y} = \frac{\partial\tilde{n}}{\partial t} + U_{dw}\frac{\partial\tilde{n}}{\partial y} = 0, \qquad \text{(VII.5)}$$

where

$$U_{dw}(x) = -\frac{cT_e}{eB}\frac{d\ell n(n)}{dx} \equiv \frac{cT_e}{eB}\Lambda_n(x). \qquad \text{(VII.6)}$$

It is easy to see that the general solution of Eq. (VII.5) can be written as $\tilde{n}(\vec{r},t) = f(y - U_{dw}t)$ and describes, in agreement with our physical picture, the wave propagating along the y coordinate (here $f(y)$ is an arbitrary function, which can also depend on both the x and z coordinates).

We notice that $\vec{U}_{dw}$ equals to the electron diamagnetic velocity, $\vec{V}_e^{dia}$, which occurs due to inhomogeneity of the electron Larmor circles and can be found from the cross-field electron momentum balance equation where the electron pressure gradient (the density gradient, for the case of constant temperature) is balanced by the Lorentz force:

$$-T_e\frac{dn(x)}{dx}\vec{e}_x - \frac{eB_0}{c}\left(\vec{V}_e^{dia}\times\vec{e}_z\right)n(x) = 0. \qquad \text{(VII.7)}$$

However, the expression for the evolution of the perturbed plasma density (VII.5) does not take into account some crucially important effects. First, in the derivation of Eq. (VII.5) we assumed that the cross-field motion of the charged particles is only due to $\vec{E}\times\vec{B}$ drift, which is the same for both electrons and ions. However, the mass difference causes an important disparity in the dynamics of the electrons and ions. It results in a more complex governing equation for the perturbed plasma density, which becomes important for both the linear stability and nonlinear interactions of the drift waves.

Secondly, and more importantly, Eq. (VI5) shows that the amplitudes of both the perturbed plasma density and electrostatic potential, linked to the density perturbation through the Boltzmann relation (VII.2), remain the same and do not grow in time. Therefore, it cannot describe instabilities resulting in large plasma density/potential fluctuations and strong cross-field anomalous transport observed in experiments.

To address the first issue we consider the equation for the ion velocity, $\vec{V}_i$, which follows from the ion momentum balance equation and in the cold ion approximation reads:

$$M\frac{d\vec{V}_i}{dt} = -e\nabla\varphi + \frac{eB}{c}\left(\vec{V}_i\times\vec{e}_z\right), \qquad \text{(VII.8)}$$

where M is the ion mass and

$$\frac{d\vec{V}_i}{dt} \equiv \frac{\partial \vec{V}_i}{\partial t} + \left(\vec{V}_i \cdot \nabla\right)\vec{V}_i \tag{VII.9}$$

is the so-called material derivative.

Since we consider the characteristic frequency $\omega << \Omega_{Bi}$, the leading cross-field term depending on the ion velocity in Eq. (VII.8) is the last one and we can find the solution for $\vec{V}_{i\perp}$ through successive approximations in the small parameter ω / Ω_{Bi}. Keeping only two terms in such an expansion and allowing for a linear approximation in the amplitude of the electrostatic potential, from Eq. (VII.8, VII.9) we find

$$\tilde{\vec{V}}_{i\perp} = -c\frac{\left(\nabla\tilde{\varphi} \times \vec{e}_z\right)}{B} - \frac{1}{\Omega_{Bi}}\frac{\partial}{\partial t}\left(c\frac{\nabla\tilde{\varphi}}{B}\right), \tag{VII.10}$$

where the second term is from the ion inertia term in Eq. (VII.8).

We notice that the inertial term on the right-hand side of Eq. (VII.10) is smaller than the first one which is already the familiar $\vec{E} \times \vec{B}$ drift velocity. However, unlike the $\vec{E} \times \vec{B}$ drift, the second term is not divergence-free.

In the linear approximation of the parallel component of the ion velocity, $\tilde{\vec{V}}_{i\parallel}$, from Eq. (VII.8) we have

$$\frac{\partial \tilde{\vec{V}}_{i\parallel}}{\partial t} = -\frac{e\nabla_\parallel \tilde{\varphi}}{M}. \tag{VII.11}$$

Then, substituting the expressions (VII.10, VII.11)) into the ion continuity equation, we have

$$\frac{\partial^2}{\partial t^2}\left\{\frac{\tilde{n}_i}{n_0} - \rho_s^2\nabla_\perp^2\tilde{\phi}\right\} - C_s^2\nabla_\parallel^2\tilde{\phi} + U_{dw}\frac{\partial^2}{\partial t \partial y}\tilde{\phi} = 0, \tag{VII.12}$$

where $C_s = \sqrt{T_e / M}$ is the ion sound speed and ρ_s is an effective ion Larmor radius, defined as $\rho_s^2 = T_e / (M\Omega_{Bi}^2)$. From Eq. (VII.12), using the Boltzmann relation (VII.2) for the electron density and assuming the quasi-neutrality condition, we obtain the following equation for the evolution of a small plasma density perturbation:

$$\frac{\partial^2}{\partial t^2}\left\{\tilde{n} - \rho_s^2\nabla_\perp^2\tilde{n}\right\} - C_s^2\nabla_\parallel^2\tilde{n} + U_{dw}\frac{\partial^2\tilde{n}}{\partial t \partial y} = 0. \tag{VII.13}$$

As we can see, unlike Eq. (VII.5), Eq. (VII.13) does not describe the advection of the perturbed plasma density in the y-direction as a whole anymore, $\tilde{n}(t,\vec{r}) = f(y - U_{dw}t)$. The reason for this is the so-called dispersion of the drift wave frequency (i.e. the dependence of the frequency ω on the wave vector $\vec{k}$, $\omega(\vec{k})$). Indeed, assuming that the wavelength in the x-direction is much smaller than the characteristic scale length of the inhomogeneity of the plasma density, $|d\ell n(n)/dx|^{-1}$, we can assume that $\Lambda_n(x) = \text{const.}$ and use the eikonal approximation [5] taking $\tilde{n} = \hat{n}_{\omega,\vec{k}} \exp(-i\omega + i\vec{k}\cdot\vec{r})$, where $\hat{n}_{\omega,\vec{k}}$ is the amplitude of the corresponding wave

packet. To simplify notations, thereafter we omit both the "hat" and the ω and $\vec{k}$ indices over and at the Fourier harmonics. Then, from Eq. (VII.5) we find

$$\omega(\vec{k}) = U_{dw} k_y \equiv \omega_* . \qquad \text{(VII.14)}$$

This simple relation gives the wave group velocity, $\partial\omega(\vec{k})/\partial\vec{k} = U_{dw}\vec{e}_y$, independent of $\vec{k}$, which means that all spatial scale lengths will be advected in the y-direction with the same speed and, therefore, the spatial shape of δn will be preserved: $\tilde{n}(t,\vec{r}) = f(y - U_{dw}t)$. But, Eq. (VII.13) yields a more complex dispersion,

$$\frac{\omega_*}{\omega} + \frac{C_s^2 k_{||}^2}{\omega^2} = 1 + \rho_s^2 k_\perp^2 , \qquad \text{(VII.15)}$$

where $\vec{k}_\perp$ and $k_{||}$ are the components of the wave vector perpendicular and parallel to the magnetic field lines. Thus, now the group velocity depends on $\vec{k}$ and, therefore, the spatial shape of $\tilde{n}(\vec{r},t)$ will change in time (e.g. in the y-direction).

The solution of Eq. (VII.15) has two important branches. For $k_{||}^2 \to 0$, Eq. (VII.15) gives the dispersion of the drift waves modified, in comparison with Eq. (VII.14), by the cross-field ion inertia:

$$\omega(\vec{k}) = \frac{\omega_*}{1 + \rho_s^2 k_\perp^2} >> C_s k_{||} , \qquad \text{(VII.16)}$$

whereas for $k_{||}^2 \to \infty$, we have the ion sound waves with

$$\omega = \frac{C_s k_{||}}{\sqrt{1 + \rho_s^2 k_\perp^2}} >> \omega_* . \qquad \text{(VII.17)}$$

We notice that the phase velocity of the ion sound waves is $\sim C_s = \sqrt{T_e / M}$. Therefore, inequalities (VII.1) for the ion sound waves only hold for $T_e >> T_i$, which is compatible with the cold ion approximation we are using here. However, in the tokamak plasmas, where usually $T_e \approx T_i$, the ion sound waves are strongly damped due to the Landau resonance with ions.

We notice that in Eq. (VII.12) we neglect the x-component of the inertial part of the cross-field ion velocity in the term $\vec{V}_{i\perp} \cdot \nabla n$ since its contribution is much smaller than that of the corresponding $\vec{E} \times \vec{B}$ drift velocity component. However, this term becomes important for the evolution of the amplitude of the wave packet. This effect can also be seen for the case of non-constant $\Lambda_n(x)$ where the drift wave can be localized within some range along the x-coordinate.

VII.2.2 Localized drift wave

In the previous consideration of the drift waves, we used the eikonal approximation where all perturbations are proportional to $\exp(ik_x x)$, which is valid for $|k_x| >> |\Lambda_n| = \text{const.}$. However, taking into account the x-dependence of Λ_n, we can also consider a drift wave where the perturbations are described by $\hat{f}(x)\exp(-i\omega t + ik_y y)$, where $\hat{f}(x)$ is some function localized in the x-direction. As an example, we consider a case of

$$n(x) = \bar{n} - \frac{\Delta n}{2}\tan h\left(\frac{x}{w}\right), \qquad \text{(VII.18)}$$

where $\bar{n}$ and Δn are constants and w is some scale-length. We assume that $\Delta n << \bar{n}$, and using the Boussinesq approximation that omits the density variation in the inertial term, neglecting the parallel ion dynamics in Eq. (VII.13), we arrive at the following differential equation for $\tilde{\phi}(x)$

$$\frac{d^2\tilde{\phi}}{dx^2} + \frac{(\hat{\omega}_* / \omega)}{\cosh^2(x/w)}\frac{\tilde{\phi}}{\rho_s^2} = \left(1 + \rho_s^2 k_y^2\right)\frac{\tilde{\phi}}{\rho_s^2}, \qquad \text{(VII.19)}$$

where $\hat{\omega}_* = \frac{cT_e}{eB}\frac{\Delta n}{2w\bar{n}}$. For a localized $\tilde{\phi}(x)$, ω should be considered an effective eigenvalue of the solution of Eq. (VII.19). We notice that Eq. (VII.19) is similar to the Schrödinger equation for an electron with effective electron energy $\propto -(1+\rho_s^2 k_y^2)$ in the potential well $\propto -ch^{-2}(x/w)$ [6]. Using the results of [6], after some algebra, we find that the solution of Eq. (VII.19) is characterized by an integer number m ($m = 0, 1, 2, \ldots$). For the $m = 0$ mode, we have the following frequency and the eigenfunction

$$\omega_{m=0} = \frac{\hat{\omega}_*}{1 + \rho_s^2 k_y^2 + K^{-1}}, \qquad \tilde{\phi}_{m=0}(x) = \cosh^{-K}(x/w), \qquad \text{(VII.20)}$$

where $K = (w/\rho_s)\sqrt{1+\rho_s^2 k_y^2}$. For $w >> \rho_s$, $\tilde{\phi}_{m=0}(x)$ can be approximated as follows

$$\tilde{\phi}_0(x) \propto \exp\left\{-K(x/\rho_s)^2\right\}, \qquad \text{(VII.21)}$$

which shows that the "localization width" of the $m = 0$ mode is $\sim \sqrt{\rho_s w} << w$.

Although the solution for a localized drift wave we consider here is somewhat idealized, it will allow us making some illustration of the impact of plasma flow velocity shear on drift wave plasma instability later.

VII.2.3 Dissipative drift wave instabilities in slab geometry

All drift wave dispersion equations we considered so far show that $\omega(\vec{k})$ is real and, therefore, no growth of initially small perturbations is possible. However, we will see that allowing for dissipative effects in the electron dynamics results in destabilization and growth of the drift wave amplitude. Such dissipative effects can be caused by both the Landau resonance of the wave with electrons (even though we assume that $\omega / k_{||} < V_{Te}$, some small, but finite effect of such a resonance is still present) and electron-ion collisions.

To allow for the impact of the Landau resonance on the drift wave (VII.16), we need to describe the electron dynamics kinetically. For our case it can be done by introducing the electron distribution function, $f_e(\vec{v}, \vec{r}, t)$, and employing the electron drift-kinetic equation (e.g. see [1], [2]), which reads:

$$\frac{\partial f_e}{\partial t} + v_{||}\frac{\partial f_e}{\partial z} - \frac{c}{B^2}\left(\nabla\varphi \times \vec{B}\right)\cdot\nabla f_e + \frac{e}{m}\nabla_{||}\varphi\frac{\partial f_e}{\partial v_{||}} = 0. \qquad \text{(VII.22)}$$

Since we consider linear perturbations, we take $f_e(\vec{v},\vec{r},t) = f_e^{(0)}(\vec{v},x) + \tilde{f}_e(\vec{v},\vec{r},t)$, where $f_e^{(0)}(\vec{v},x)$ is the initial electron distribution function and $\tilde{f}_e(\vec{v},\vec{r},t) \propto \exp(-i\omega t + i\vec{k}\vec{r})$ is a small correction. Then from Eq. (VII.22) we find the following expression for the electron density perturbation, $\tilde{n}_e = \int \tilde{f}_e(\vec{v},\vec{r},t)d\vec{v}$:

$$\tilde{n}_e = \tilde{\varphi}\int\left(-\frac{ck_y}{B_0}\frac{\partial f_e^{(0)}}{\partial x} + \frac{ek_{||}}{m}\frac{\partial f_e^{(0)}}{\partial v_{||}}\right)\frac{d\vec{v}}{\omega - k_{||}v_{||}}. \qquad \text{(VII.23)}$$

Assuming that $f_e^{(0)}(\vec{v},x)$ is Maxwellian, $f_{e,M}^{(0)}(\vec{v},x) \equiv n(x)\left(\sqrt{2\pi}V_{Te}\right)^{-3}\exp\left(-v^2/2V_{Te}^2\right)$, we find that Eq. (VII.23) can be re-written as

$$\tilde{n}_e = \tilde{\phi}\int\frac{(\omega_* - k_{||}v_{||})f_{e,M}^{(0)}(\vec{v},x)d\vec{v}}{\omega - k_{||}v_{||}}. \qquad \text{(VII.24)}$$

From Eq. (VII.24) we see that due to inhomogeneity of the plasma density and $\vec{E}\times\vec{B}$ drift, the sign of the effective derivative of the electron distribution function at the resonance condition $\omega = k_{||}v_{||}$ changes from being negative for the Maxwellian function to positive in Eq. (VII.24) for $\omega < \omega_*$. Therefore, according to the standard interpretation of Landau mechanism of the wave damping/growth (e.g. recall "the bump on tail instability" caused by the Landau resonance, see Ref. [7]), in our case, the amplitude of the drift wave having $\omega < \omega_*$ (recall expression VII.16) will grow. It also tells us that the energy needed for such growth comes from the electron kinetic energy.

To find a quantitative expression for the growth rate, from Eq. (VII.24) we find

$$\frac{\tilde{n}_e}{n} = \tilde{\phi}\left\{1 + \frac{\omega - \omega_*}{\sqrt{2}k_{||}V_{Te}}Z\left(\frac{\omega}{\sqrt{2}k_{||}V_{Te}}\right)\right\}, \qquad \text{(VII.25)}$$

where $Z(\varsigma)$ is the plasma dispersion function:

$$Z(\varsigma) = \frac{1}{\sqrt{\pi}}\int_{-\infty}^{\infty}\frac{d\xi\exp(-\xi^2)}{\xi - \varsigma} = \exp(-\varsigma^2)\left(i\sqrt{\pi} - 2\int_0^{\varsigma}d\xi\exp(\xi^2)\right). \qquad \text{(VII.26)}$$

For $\omega << k_{||}V_{Te}$, from Eq. (VII.25) we obtain the following expression for the electron density perturbation

$$\frac{\tilde{n}_e}{n} = \frac{e\tilde{\varphi}}{T_e}\left\{1 + i\sqrt{\frac{\pi}{2}}\frac{\omega - \omega_*}{k_{||}V_{Te}}\right\}, \qquad \text{(VII.27)}$$

which, due to the Landau resonance, is slightly different from the Boltzmann relation we have used so far. Then, recalling Eq. (VII.12) and using the quasi-neutrality conditions, we arrive at the following dispersion equation

$$\frac{\omega_*}{\omega} + \frac{C_s^2k_{||}^2}{\omega^2} = 1 + \rho_s^2k_{\perp}^2 + i\sqrt{\frac{\pi}{2}}\frac{\omega - \omega_*}{k_{||}V_{Te}}. \qquad \text{(VII.28)}$$

Since we assume $\omega << k_{||}V_{Te}$, the last term on the right-hand side of Eq. (VII.28) is below unity, but this is the only term that gives a complex expression for the solution of the dispersion equation (VII.28). As a result, for the drift waves, this term gives

$$\omega = \frac{\omega_*}{1+k_\perp^2\rho_s^2}\left\{1+i\sqrt{\frac{\pi}{2}}\frac{\omega_*}{k_{||}V_{Te}}k_\perp^2\rho_s^2\left(1+k_\perp^2\rho_s^2\right)^{-2}\right\}, \qquad \text{(VII.29)}$$

and the frequency has a positive imaginary part, $\mathrm{Im}(\omega) > 0$, which implies that the amplitude of the perturbation, $\propto \exp(-i\omega + i\vec{k}\cdot\vec{r}) \propto \exp(\mathrm{Im}(\omega)t)$, will grow exponentially with time. At the same time, for the ion sound waves having $\omega > \omega_*$, the last term in Eq. (VII.28) results in collisionless damping.

Next, we consider the impact of electron-ion collisions on destabilization of the drift waves described by Eq. (VII.14). For this purpose we will use the plasma fluid equations (e.g. see [8], [9], [10], [11], [12]). As we already found, the drift waves cause some perturbation of the electron distribution function. In terms of the fluid equations, in the presence of collisions, the drift waves will result in the perturbation not only of the plasma density but also of the electron temperature (we will still consider the cold ion approximation and ignore electron energy dissipation due to electron-ion collisions). Then, from the electron fluid momentum and energy equations, omitting rather cumbersome algebra, we find (e.g. see [13])

$$\frac{\tilde{n}_e}{n} = \frac{e\tilde{\varphi}}{T_e}\left\{\frac{(\omega_* + i\nu_{||})(3\omega/2 + i\kappa\nu_{||}) + i(1+\alpha_T)\omega_*\nu_{||}}{(\omega + i\nu_{||})(3\omega/2 + i\kappa\nu_{||}) + i(1+\alpha_T)\omega\nu_{||}}\right\}, \qquad \text{(VII.30)}$$

where $\nu_{||} = k_{||}^2(T_e/m\nu_{ei})$ plays the role of the inverse characteristic time of electron diffusion on the spatial scale $\sim k_{||}^{-1}$, ν_{ei} is the electron-ion collision frequency, $\kappa = 1.61$ and $\alpha_T = 0.71$. We notice that the terms proportional to κ and $1+\alpha_T$ come, respectively, from the contribution of the electron temperature perturbation to heat conduction and from the momentum balance equations along the magnetic field lines where α_T describes the electron thermal force effect.

For the case $\nu_{||} >> \omega_*$, when the electron density perturbation can be described with the Boltzmann relation, from Eq. (VII.30) we have

$$\frac{\tilde{n}_e}{n} = \tilde{\phi}\left\{1+i\frac{\omega-\omega_*}{\nu_{||}}\left(1+\frac{1+\alpha_T}{\kappa}\right)\right\}. \qquad \text{(VII.31)}$$

As one can see, similarly to the collisionless Landau dissipation (VII.27), the imaginary part of the expression (VII.31) is also proportional to the difference $\omega - \omega_*$, which results in instability for the case of the drift wave:

$$\omega \approx \frac{\omega_*}{1+\rho_s^2k_\perp^2}\left\{1+i\frac{\omega_*}{\nu_{||}}\rho_s^2k_\perp^2\left(1+\rho_s^2k_\perp^2\right)^{-2}\left(1+\frac{1+\alpha_T}{\kappa}\right)\right\}. \qquad \text{(VII.32)}$$

where the frequency, similar to Eq.(VII.29), has a positive imaginary part proportional to $\rho_s^2k_\perp^2$. We notice that from Eq. (VII.32) one can see that the omission of the electron temperature

variation (which formally corresponds to the case of $\kappa \to \infty$) would only give an order of unity correction for the growth rate.

But, we should keep in mind that the applicability of the fluid equations for the study of the dissipation effects caused by electron-ion collisions on the stability of the drift waves requires a relatively slow spatiotemporal variation of plasma parameters: $k_{||}V_{Te}/\nu_{ei} \equiv k_{||}\lambda_{Ce} << 1$ and $\omega/\nu_{ei} << 1$, where λ_{Ce} is the electron mean free path. Therefore, the inequality $\nu_{||} >> \omega_*$ that we used to derive Eq. (VII.31) requires the following conditions: $\omega/\nu_{ei} << \left(k_{||}V_{Te}/\nu_{ei}\right)^2 << 1$. For a more general case, the contributions of both the Landau resonance and electron-ion collisions to the growth-rate can be comparable even for $\omega/\nu_{ei} < 1$ [13].

For $\nu_{||} \to 0$, which corresponds to slow relaxation of the electron density perturbation along the magnetic field lines, from Eq. (VII.30) we have

$$\frac{\tilde{n}_e}{n} = \tilde{\phi}\left\{\frac{\omega_*}{\omega} + \frac{i\nu_{||}}{\omega}\left(1 - \frac{\omega_*}{\omega}\right)\right\}. \qquad \text{(VII.33)}$$

Then, neglecting in Eq.(VII.12) the ion dynamics along the magnetic field, from the quasi-neutrality conditions we find the following dispersion equation

$$\rho_s^2 k_\perp^2 + \frac{i\nu_{||}}{\omega}\left(1 - \frac{\omega_*}{\omega}\right) = 0, \qquad \text{(VII.34)}$$

which for $\nu_{||} \to 0$, has an unstable solution with

$$\omega = (1+i)\sqrt{\frac{\nu_{||}\omega_*}{2\rho_s^2 k_\perp^2}}. \qquad \text{(VII.35)}$$

The fact that $\omega(\nu_{||} \to 0) \to 0$ is not surprising if we recall that the wave is driven by the electric field, which is due to plasma polarization related to electron mobility along the magnetic field lines (see Fig. VII.1) and such mobility is strongly suppressed for the case of $\nu_{||} \to 0$.

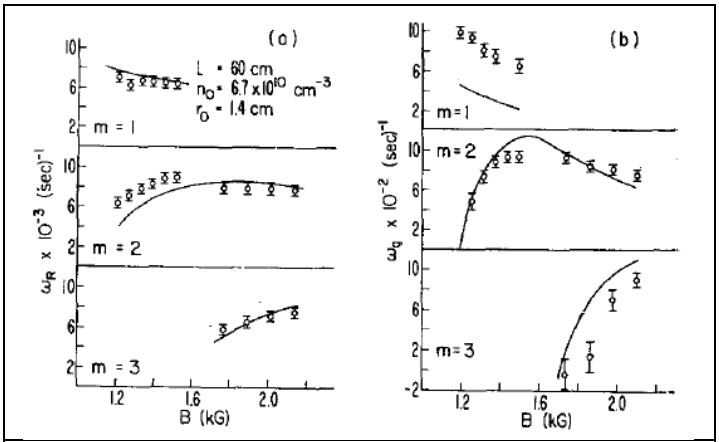

Fig. VII.2. Comparison of experimental data (dots) and theoretical calculations (solid curves) for collisional drift wave frequency (left) and growth rate (right) for different azimuthal wave numbers m. Reproduced with permission from [19], © AIP Publishing 1970.

The basic features of both the collisionless and collisional drift waves in a non-tokamak environment were extensively studied in the 1960th-1970th (e.g. see Ref. [14], [15], [16], [17], [18] and the references therein). Due to relatively quiescent and controllable plasmas in the devices used in these studies (in many cases these were the Q-machines, with the straight magnetic field lines where the plasma was created by the ionization of cesium or potassium atoms at the

surface of a hot plate) a reasonable agreement was found between the theoretical expectations and the experimental data for the case of low wave amplitudes, where the linear wave theory is valid. For example, in Fig. VII.2 one can see a good agreement between the experimental data and theoretical calculations for the collisional drift wave frequency and growth rate for different azimuthal wavenumbers m. The situation with experimental studies of the drift waves in toroidal devices, where the plasma waves can be simultaneously driven by different mechanisms, is not so obvious and largely only qualitative agreement between the results of the drift wave theory and the experimental observations is reported (e.g. see [20], [4], [21], [22] and the references therein).

VII.2.4 Destabilizing effect of ion temperature gradient

However, it appears that the presence of a cross-field ion temperature gradient can result in plasma instability with no dissipation effects. In this case, another kind of drift wave, the so-called ion temperature gradient (ITG) drift mode [23] can become unstable.

As an example, we consider plasma with homogeneous both density and electron temperature embedded into a constant magnetic field $\vec{B}_0 = B_0\vec{e}_z$ but having the ion temperature depending on the x-coordinate, $\partial T_i / \partial x \neq 0$.

Then, the ion $\vec{E}\times\vec{B}$ drift will result in a perturbation of the ion temperature, $\tilde{T}_i$, similar to that of the plasma density described by Eq. (VII.4):

$$\frac{\partial}{\partial t}\left(\frac{\tilde{T}_i}{T_i}\right) + U_{dw,i}\frac{\partial\tilde{\phi}}{\partial y} = 0\,, \qquad \text{(VII.36)}$$

where

$$U_{dw,i} = -\frac{cT_e}{eB_0}\frac{d\ell n(T_i)}{dx}\,. \qquad \text{(VII.37)}$$

For the case of $k_{||} \neq 0$, the perturbation of the ion temperature $\tilde{T}_i$ results in the perturbation of the plasma pressure along the magnetic field lines, which is somewhat similar to the plasma density inhomogeneity along the magnetic field shown in Fig. VII.1.

Standard wisdom would suggest that the perturbation of plasma pressure should result in some sort of a "sound" wave, similar to the ion sound waves, Eq. (VII.17), with $\omega \sim C_p k_{||}$, where C_p is the plasma sound speed. Although this option exists, we consider a very different regime of the ion dynamics, which will finally bring us to the unstable ITG mode. Following Eq. (VII.1) we assume that $\omega >> V_{T_i} k_{||}$. We will see that such inequality becomes possible because in inhomogeneous plasma, among different characteristic frequencies of the waves there are drift frequencies such as $\omega_* = U_{dw} k_y$ (Eq. (VII.12)) and, as we will see,

$$\omega_{*,i} = U_{dw,i} k_y\,, \qquad \text{(VII.38)}$$

which do not depend on $k_{||}$.

Then, the ion dynamics can be considered as a motion under a "fast" ($\omega >> V_{T_i} k_{||}$) applied force caused by the ion temperature perturbation. As a result of such forced ion motion,

the perturbations of both the plasma density and electrostatic potential will be relatively small but vital for the instability:

$$\frac{e\tilde{\varphi}}{T_i} \sim \frac{\tilde{n}_i}{n} << \frac{\tilde{T}_i}{T_i}. \qquad \text{(VII.39)}$$

We assume here that $T_e \sim T_i$. Then, from ion momentum balance along the magnetic field and the continuity equations we have

$$\frac{M}{T_i}\frac{\partial^2}{\partial t^2}\left(\frac{\tilde{n}_i}{n}\right) = \nabla_{||}^2\left(\frac{\tilde{T}_i}{T_i}\right), \qquad \text{(VII.40)}$$

which demonstrates that for $\omega >> V_{T_i} k_{||}$,

$$\frac{\tilde{\varphi}}{T_i} \sim \frac{\tilde{n}_i}{n} = \left(\frac{V_{T_i} k_{||}}{\omega}\right)^2 \frac{\tilde{T}_i}{T_i} << \frac{\tilde{T}_i}{T_i}, \qquad \text{(VII.41)}$$

and justifies the inequalities (VII.39).

As a result, using the Boltzmann relation for the electron density perturbation and re-writing all our expressions in the Fourier representation, from Eq. (VII.36, VII.40) we find

$$\omega^3 = \omega_{*,i} k_{||}^2 V_{T_i}^2. \qquad \text{(VII.42)}$$

This third-order equation for ω has one real and two complex conjugate solutions, which ensures the existence of the solution with the positive imaginary part of ω, which implies the instability of this ITG mode.

We notice that in our derivation, among other assumptions we presumed that $\omega >> V_{T_i} k_{||}$, which, as one can see from Eq. (VII.39), is satisfied for relatively small $k_{||}$: $\omega_{*,i} >> V_{T_i} k_{||}$, so that the growth rate of the instability described by Eq. (VII.42) is significantly below $\omega_{*,i}$.

VII.2.5 Plasma instabilities driven by toroidal effects

So far we considered plasma in a straight constant magnetic field. However, in a tokamak, the magnetic field $\vec{B}$ has a helical structure winding around toroidally symmetric magnetic flux surfaces (see Fig. I.1). As a result, any charged particle having a reasonably small Larmor radius will experience cross-$\vec{B}$ drift motion associated with both the curvature of the magnetic field lines and the gradient of the magnetic field strength.

In a tokamak having a large aspect ratio (the ratio of major to minor tokamak radii), both these drifts are largely determined by the toroidal magnetic field, $\vec{B}_{tor}$, and the velocities of these drifts are directed along the major tokamak axis. For this case, the average magnetic field-related drift velocity of an ensemble of the particles having a charge q and a Maxwellian distribution function with the temperature T_q can be written as

$$\vec{V}_{B,q} = 2\frac{cT_q}{qB}\frac{(\vec{e}_R \times \vec{b})}{R}. \qquad \text{(VII.43)}$$

Here we use cylindrical coordinates (Z,R,ϕ) where the Z coordinate goes along the major tokamak axis, whereas $\vec{e}_R$ is the unit vector along the R coordinate, $\vec{b}=\vec{B}/B$, and assume $B_{tor}\propto 1/R$.

We notice that the direction of $\vec{V}_B$ depends on the sign of the charge so that the electrons and ions drift in opposite directions. As a result, a radial protrusion of the plasma parameters can cause plasma polarization not only due to the electron motion along the magnetic field as shown in Fig. VII.1, but also due to the magnetic field-related drifts of the electrons and ions. As a result of such plasma polarization, new types of instabilities become possible.

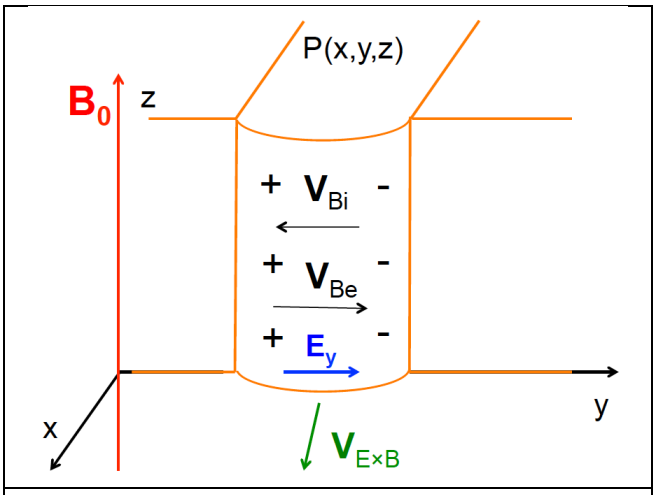

Fig. VII.3. The magnetic drift-related polarization of plasma pressure protrusion and associated $\vec{E}\times\vec{B}$ plasma drift that can result in further radial advection of the protrusion.

As an example, in Fig. VII.3 we show magnetic drift-related polarization of a plasma pressure protrusion which, unlike those in Fig. VII.1, is not inclined to the direction of the magnetic field lines. As one can see, in this particular case, a dipole-like polarization of the plasma pressure protrusion due to the magnetic drift and associated $\vec{E}\times\vec{B}$ plasma drift can result in further radial advection of the protrusion.

However, we notice that the drift velocities Eq. (VII.40) appear only in the motion of test particles. Within the fluid picture of the plasma dynamics, these velocities are "hidden" in the diamagnetic velocities of plasma components, $\vec{V}_{e/i}^{dia}$, which, in the presence of toroidal effects, can result in non-divergence-free perturbations of the electron/ion fluxes. Indeed, the cross-field diamagnetic flux, $\vec{j}_q^{dia}$, of an ensemble of particles with charge q and pressure P_q is

$$\vec{j}_q^{dia}=\frac{c}{q}\frac{\vec{B}\times\nabla P_q}{B^2}. \qquad \text{(VII.44)}$$

Then, assuming $B\propto 1/R$, from Eq. (VII.44) we find

$$\nabla\cdot\vec{j}_q^{dia}=-\frac{2c}{qB}\frac{\vec{b}\cdot\left(\vec{e}_R\times\nabla P_q\right)}{R}. \qquad \text{(VII.45)}$$

A similar result can be found from the divergence of the flux $n_q\vec{V}_{B,q}$.

Another implication of the spatial variation of the magnetic field is that the $\vec{E}\times\vec{B}$ drift velocity is also no longer divergence-free even for the potential electric field $\vec{E}=-\nabla\varphi$. Indeed, assuming that $B\propto 1/R$, for this case from Eq. (VII.3) we find

$$\nabla\cdot\vec{V}_{\vec{E}\times\vec{B}}=\frac{2c}{B}\vec{b}\cdot\left(\nabla\ell n(B)\times\nabla\varphi\right)=-\frac{2c}{B}\frac{\vec{b}\cdot\left(\vec{e}_R\times\nabla\varphi\right)}{R}. \qquad \text{(VII.46)}$$

Although in large aspect ratio ($R>>a$) tokamaks $|V_{B,q}|$ is relatively small

$$|V_{B,q}| \propto \frac{1}{R} << |U_{dw}|, |U_{dw,i}| \propto \frac{1}{a}, \tag{VII.47}$$

the cross-field drift velocity $\vec{V}_B$ can cause plasma polarization (recall Fig. VII.2), which, as we will see, results in a new class of plasma instabilities. In what follows, along with the frequencies ω_* and $\omega_{*,q}$, we will use frequencies $\omega_{B,q} = \vec{V}_{B,q} \cdot \vec{k}$, which, according to Eq. (VII.47), have the following ordering

$$|\omega_{B,q}| << \omega_*, \omega_{*,q}. \tag{VII.48}$$

As an example, we consider the impact of a weakly toroidal magnetic field on the ITG mode. We introduce a local coordinate system (x,y,z), where x, y, and z are in the radial, poloidal, and $\vec{B}$ directions respectively and, as we did before, take constant plasma density and electron temperature and assume that the ion temperature is varying in the "radial" direction: $\partial T_i / \partial x \neq 0$.

We recall that for the case of a constant magnetic field, the only reason for establishing the perturbations of the plasma density and corresponding electrostatic potential was the ion motion along the magnetic field caused by the ion temperature (pressure) perturbation. However, in the presence of toroidal effects, perturbation of the ion temperature (pressure) results in a finite divergence of the diamagnetic ion flux (VII.45) and, therefore, in the ion density perturbation. To emphasize the toroidal effects, we completely neglect here the impact of the ion dynamics along the magnetic field lines and the effects of the ion inertia. We will be interested in plasma fluctuations with the frequency ω such that

$$|\omega_{B,q}| < \omega < \omega_*, \omega_{*,q}. \tag{VII.49}$$

Then we will see that in our case, the ion temperature has the largest relative perturbation and, similarly to Eq. (VII.41), $\tilde{T}_i / T_i >> \tilde{\phi} \sim \tilde{n}_i / n_0$ (we assume here $T_i \sim T_e$). As a result, the ion temperature perturbation can still be described by Eq. (VII.36), which gives

$$\frac{\tilde{T}_i}{T_i} = \frac{\omega_{dw,i}}{\omega} \tilde{\phi}. \tag{VII.50}$$

Finding $\tilde{n}_i$ we can allow for the ion temperature perturbation in the ion diamagnetic flux (VII.44) only and neglect the compressibility of the $\vec{E} \times \vec{B}$ drift flow since $\tilde{T}_i / T_i >> \tilde{\phi}$. So we have

$$\frac{\tilde{n}_i}{n_0} = \frac{\omega_{B,i}}{\omega} \frac{\tilde{T}_i}{T_i}. \tag{VII.51}$$

Assuming the Boltzmann relation for the electron density perturbation and electrostatic potential together with the plasma quasi-neutrality from Eq. (VII.50, VII.51), we find

$$\omega^2 = \omega_{*,i} \omega_{B,i} \equiv 2 \frac{T_i}{T_e} \left(\frac{cT_e}{eB_0} \right)^2 \frac{k_y^2}{R} \frac{d\ell n(T_i)}{dx}, \tag{VII.52}$$

which satisfies the inequality (VII.49) and all other assumptions made in the course of our derivation of Eq. (VII.52) and shows the instability of the toroidal ITG for $\partial T_i / \partial x < 0$.

However, we notice that x is the local coordinate and for the "standard" temperature distribution over the minor radius, $\partial T_i / \partial x < 0$ region corresponds to the outboard side of the torus (or to the so-called "bad" curvature region), whereas at the inboard side (where the curvature is "good") $\partial T_i / \partial x > 0$ and the mode is neutrally stable (within our simplified treatment).

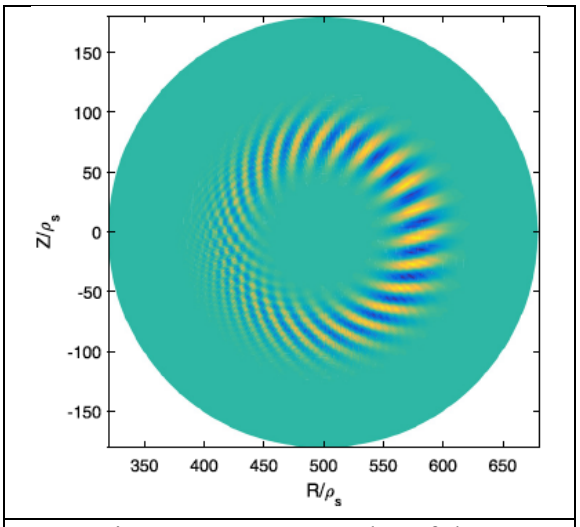

Fig. VII.4. Contour plot of the eigenfunction of electrostatic potential at some toroidal cross-section found for ITG mode. Reproduced with permission from [24], © AIP Publishing 2017.

Eq. (VII.52) gives the growth rate of the ITG instability in the eikonal approximation. More complex numerical simulations go beyond the eikonal approximation and treat the solution of the corresponding differential equations as an eigenfunction-eigenvalue problem. As a result, such solutions allow visualizing the mode structure (somewhat similar to what we did for a nonlocal solution of the drift wave arriving at Eq. (VII.20, VII.21)). As an example, in Fig. VII.4 one can find the spatial structure of the eigenfunction of the electrostatic potential at some toroidal angle found for the ITG mode. We notice that in agreement with our simplified consideration, the amplitude of the electrostatic potential shows a strong enhancement at the outer side of the torus, where, according to Eq. (VII.52), the driving mechanism is localized. However, at relatively high radial gradients of the plasma parameters, the spatial structure of the most unstable ITG eigenmode can be very different (e.g. see [25], [26] and the references therein).

VII.2.6 Interchange and resistive interchange modes

Apart from the impact on the ITG instability, the magnetic drift also brings new features to the instability of the collisional drift waves we have considered for the case of a constant magnetic field (see Eq. (VII.32, VII.35)). To asses them, we will again use a local coordinate system (x,y,z), where x, y, and z are in the radial, poloidal, and $\vec{B}$ directions respectively.

However, this time instead of finding expressions for the electron and ion density perturbations and then using the quasi-neutrality condition, we will employ the so-called vorticity equation, which is widely used, in particular, in nonlinear simulations of plasma turbulence. The vorticity equation actually follows from the quasi-neutrality conditions written in the form $\nabla \cdot \vec{J} = 0$, where $\vec{J}$ is the electric current in the plasma. In highly magnetized plasmas, the cross-field plasma current produced by fluctuating plasma parameters is only due to the ion inertia, $\tilde{\vec{J}}_\perp^{inert}$ (e.g. recall the expression (VII.10)), and diamagnetic current, $\tilde{\vec{J}}_\perp^{dia}$, associated with the electron/ion diamagnetic fluxes (VII.44). We notice that i) the $\vec{E} \times \vec{B}$ drift velocities which are the same for electrons and ions, do not contribute to cross-field electric current in a quasi-neutral plasma, and ii) $\nabla \cdot \tilde{\vec{J}}_\perp^{dia} \neq 0$ only for the case where $\vec{B}$ is not constant (e.g. recall expression (VII.45)).

For the case of the cold ion approximation, neglecting the variation of the magnetic field, from Eq. (VII.8, VII.9) we find

$$\nabla\cdot\vec{J}_{\perp}^{inert}=-e\nabla\cdot\left\{n\left(\frac{\partial}{\partial t}+\vec{V}_{\vec{E}\times\vec{B}}\cdot\nabla\right)\frac{c\nabla\tilde{\varphi}}{B\Omega_{Bi}}\right\}, \tag{VII.53}$$

whereas from Eq. (VII.45) we have

$$\nabla\cdot\vec{J}_{\perp}^{dia}=-\frac{2c}{B}\frac{\vec{b}\cdot\left(\vec{e}_R\times\nabla\tilde{P}_{tot}\right)}{R}, \tag{VII.54}$$

where $\tilde{P}_{tot}$ is the perturbation of the total plasma pressure.

Quite often Eq. (VII.53) is considered in the Boussinesq approximation where the expression (VII.53) is simplified as follows:

$$\nabla\cdot\vec{J}_{\perp}^{inert}=-en\left\{\left(\frac{\partial}{\partial t}+\vec{V}_{\vec{E}\times\vec{B}}\cdot\nabla\right)\frac{c\nabla^2\varphi}{B\Omega_{Bi}}\right\}. \tag{VII.55}$$

For linear theory, such approximation is equivalent to the omission of the inertial part of the cross-field ion velocity in the term $\vec{V}_{i\perp}\cdot\nabla n$ in Eq. (VII.12). Then, the linear vorticity equation reads

$$\nabla\cdot\tilde{\vec{J}}\equiv-en\frac{\partial}{\partial t}\frac{c\nabla^2\tilde{\varphi}}{B\Omega_{Bi}}-\frac{2c}{B}\frac{\vec{b}\cdot\left(\vec{e}_R\times\nabla\tilde{P}_{tot}\right)}{R}+\nabla_{||}\cdot\tilde{J}_{||}=0. \tag{VII.56}$$

To simplify our algebra, we will assume that the electron temperature is constant (which gives an order of unity correction for the growth rate, recall Eq. (VII.32)) so that for the perturbed electron pressure we take $\tilde{P}_e=\tilde{n}T_e$.

Finding the parallel component of the electric current, $\tilde{J}_{||}$, we will ignore the ion dynamics along the magnetic field lines. Then, assuming $\omega/\nu_{ei}<1$, from the parallel electron momentum balance equation in linear approximation we have

$$\nabla_{||}\cdot\tilde{J}_{||}=en\nu_{||}\left(\tilde{\phi}-\frac{\tilde{n}}{n}\right). \tag{VII.57}$$

First, we consider the case of $\nu_{||}\to 0$, which corresponds to reduced electron mobility along the magnetic field lines and in the absence of toroidal effects, results in a relatively slow instability (VII.35). However, toroidal effects, causing magnetic drifts, provide plasma polarization which is not related to electron mobility along the magnetic field lines and, therefore, is not bounded by the small magnitude of $\nu_{||}$. Therefore, in the simplest case, we can take $J_{||}=0$ and relax Eq. (VII.56) to

$$\rho_s^2k_{\perp}^2\frac{\partial}{\partial t}\frac{e\tilde{\varphi}}{T_e}-\frac{2cT_e}{eBR}\frac{\partial}{\partial y}\frac{\tilde{n}}{n}=0. \tag{VII.58}$$

The variation of plasma density can be found from the ion continuity equation. Considering the case $\rho_s^2k_{\perp}^2<1$ and recalling the inequality (VII.48), we can neglect the compressibility in both the inertial and $\vec{E}\times\vec{B}$ ion drift flows and use Eq. (VII.4) for the plasma density perturbation. As a result, we arrive at the following equation

$$k_\perp^2\tilde{\phi} - \frac{2T_e}{MR}\frac{k_y^2}{\omega^2}\frac{\partial \ell n(n)}{\partial x}\tilde{\phi} = 0\,, \qquad \text{(VII.59)}$$

which gives the growth rate of the so-called ideal interchange instability γ_I (e.g. see [2]):

$$\omega^2 = -\gamma_I^2 \equiv -\frac{\omega_* \omega_{B,e}}{\rho_s^2 k_\perp^2} \sim \frac{2T_e}{MR}\frac{d\ell n(n)}{dx}\,, \qquad \text{(VII.60)}$$

which, similar to the toroidal ITG mode, can only be unstable at the outboard side of the torus.

The physics of the ideal interchange instability is simple: the magnetic drift causes polarization of a plasma protrusion similar to that shown in Fig. VII.2, which, in the absence of charge relaxation along the magnetic field lines, results in a continuous build-up of the electric field and increasing amplitude of the protrusion. We notice that the ideal interchange mode has a deep analogy with the Rayleigh-Taylor instability of a stratified fluid in a gravity field (e.g. see [27]). Indeed, considering an incompressible fluid situated in a gravity field characterized by the acceleration $\vec{g} = g\vec{e}_x$ (where $g > 0$) and having the mass density $\rho(x)$, we can find the following equation describing the stream function, $\tilde{\psi}(x,y,t)$, which defines the perturbation of the fluid velocity, $\tilde{\vec{V}} = \vec{e}_z \times \nabla\tilde{\psi}$,

$$\frac{d^2\tilde{\psi}}{dx^2} - k_y^2\tilde{\psi} + \frac{1}{\rho}\frac{d\rho}{dx}\frac{gk_y^2}{\omega^2}\tilde{\psi} = 0\,. \qquad \text{(VII.61)}$$

Here we adopt the Boussinesq approximation and use the Fourier expansion of $\tilde{\psi}$ in time and y-coordinate. Then, using the eikonal approximation in the x-direction, from Eq. (61) we obtain

$$k_\perp^2\tilde{\psi} - \frac{d\ell n(\rho)}{dx}\frac{gk_y^2}{\omega^2}\tilde{\psi} = 0\,, \qquad \text{(VII.62)}$$

which is similar to Eq. (VII.59) so that we can see that the factor $2T_e / MR$ plays the role of effective gravitational acceleration for the plasma situated in a toroidal magnetic field.

By specifying the plasma density (the fluid mass density) profile from Eq. (VII.61), one can find the localized solutions of the Rayleigh-Taylor (interchange) unstable modes. For example, similarly to Eq. (VII.18), we consider the case

$$\rho(x) = \bar{\rho} - \frac{\Delta\rho}{2}\tan h\left(\frac{x}{w}\right), \qquad \text{(VII.63)}$$

where $\Delta\rho / \bar{\rho} << 1$. Here again, we use the analogy of Eq. (VII.61) to the Schrödinger equation for an electron in a potential well $\propto -ch^{-2}(x/w)$ [6] with the energy $\propto -k_y^2$, and can find the Rayleigh-Taylor (interchange) instability growth rate, γ_{RT_m}, versus the integer mode number m.

For the fastest-growing mode $m = 0$, we have the following dependence of $\gamma_{RT_{m=0}}$ and the corresponding eigenfunction, $\psi_{m=0}(x)$, on k_y:

$$\gamma_{RT_{m=0}}^2 = \bar{\gamma}_{RT}^2\frac{w|k_y|}{w|k_y|+1}, \qquad \psi_{m=0}(x) = ch^{-w|k_y|}(x/w)\,, \qquad \text{(VII.64)}$$

where

$$\bar{\gamma}_{RT}^2 = \frac{\Delta\rho}{2\bar{\rho}}\frac{g}{w}\,. \qquad \text{(VII.65)}$$

Although this solution for the Rayleigh-Taylor (interchange) instability was considered for somewhat idealized conditions, we will use it later to illustrate an impact of fluid (plasma) flow velocity shear on the Rayleigh-Taylor (interchange) instability.

Coming back to the plasma and analyzing the dissipation from Eq. (VII.56, VII.57) for $\rho_s^2 k_\perp^2 < 1$ and finite, although still rather small $\nu_{||}$, $\nu_{||} < \omega_*$, we arrive at the following modification of Eq. (VII.34):

$$\omega^2 + \gamma_I^2 + \frac{i\nu_{||}}{\rho_s^2 k_\perp^2}(\omega - \omega_*) = 0\,. \qquad \text{(VII.66)}$$

For the case of $\nu_{||} > \omega_{B,e}, \rho_s^2 k_\perp^2 \omega_*$, this gives the so-called resistive interchange mode

$$\omega = \omega_* + i\frac{\omega_{B,e}\omega_*}{\nu_{||}}\,, \qquad \text{(VII.67)}$$

which can be considered as a proxy for the "Resistive Ballooning Mode" (RBM) (e.g. see Refs. [28], [29], [30], [31], [32] and the references therein). The eigenmode structure of the RBM, found from numerical simulation for the DIII-D magnetic configuration, is shown in Fig. VII.5. Once again, one can see that the mode is largely localized at the outboard side of the torus (the "bad" curvature side).

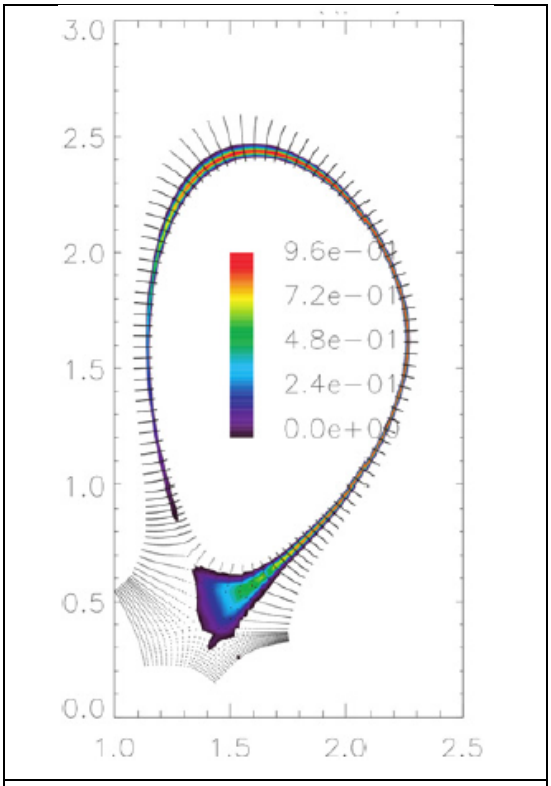

Fig. VII.5. Eigenmode structure of the RBM for the DIII-D magnetic configuration found from numerical simulation. Reproduced with permission from [33], © Elsevier 2011.

We notice that in the context of our consideration of collisional drift waves in a tokamak-like magnetic field, the term "ideal interchange mode" may sound strange. However, as we have already seen (and will see later), some dispersion equations can be rather general and, in different limits, describe different waves (e.g. recall Eq. (VII.15) which describes both the ion sound and drift waves). Similarly, considering different magnitudes of $\nu_{||}$ (which depends not only on the plasma collisionality but also on the parallel wavelength), our dispersion equation can describe different modes ranging from an unstable drift wave for large $\nu_{||}$ (recall Eq. (VII.32)) to the "ideal interchange mode" (Eq. (VII.59)) for small $\nu_{||}$.

As we see, different modes of plasma waves, coming virtually from the same set of the equations, correspond to different relations of the plasma and wave parameters. In the tokamak environment, these modes often either co-exist or are "separated" by a relatively small variation of the plasma parameters. As a result, a much more sophisticated theoretical analysis and numerical simulations, which go well beyond our basic survey, are needed to adequately describe them.

Needless to say that in experiments it is often difficult to distinguish the impacts of different modes on anomalous plasma transport. Nonetheless, as an example, in Fig. VII.6, one can see how electron temperature variation at the edge of the HL-2A tokamak switches excitation of the ITG and resistive ballooning modes (here GAM stands for the Geodesic Acoustic Mode, which is a specific, toroidally symmetric mode in a tokamak, see [35], [36] and the references therein).

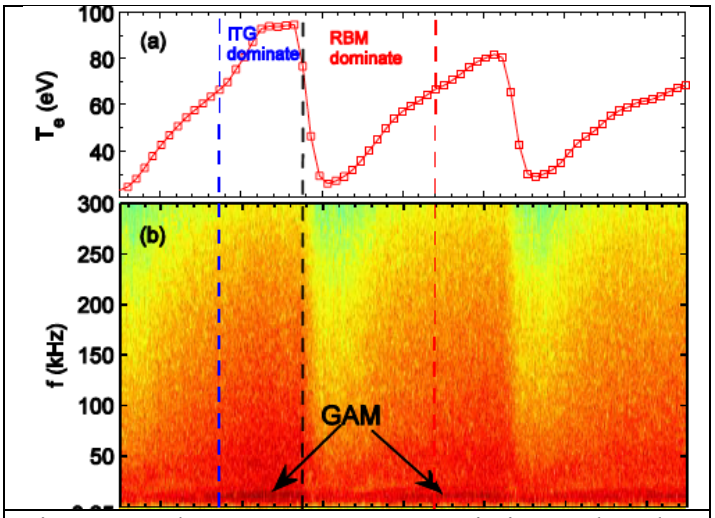

Fig.VII.6. Electron temperature variation at the edge of tokamak HL-2A tokamak (upper panel) switches back and fours the ITG and resistive ballooning modes (low panel). Reproduced with permission from [34], © IAEA 2018.

Another example can be found in [22], where the resistive drift waves and the resistive interchange mode limit of the resistive drift mode (driven by magnetic drifts) were observed correspondingly at the High Field Side (HFS) inboard and Low Field Side (LFS) outboard sides of the Helimak toroidal device, see Fig. VII.7.

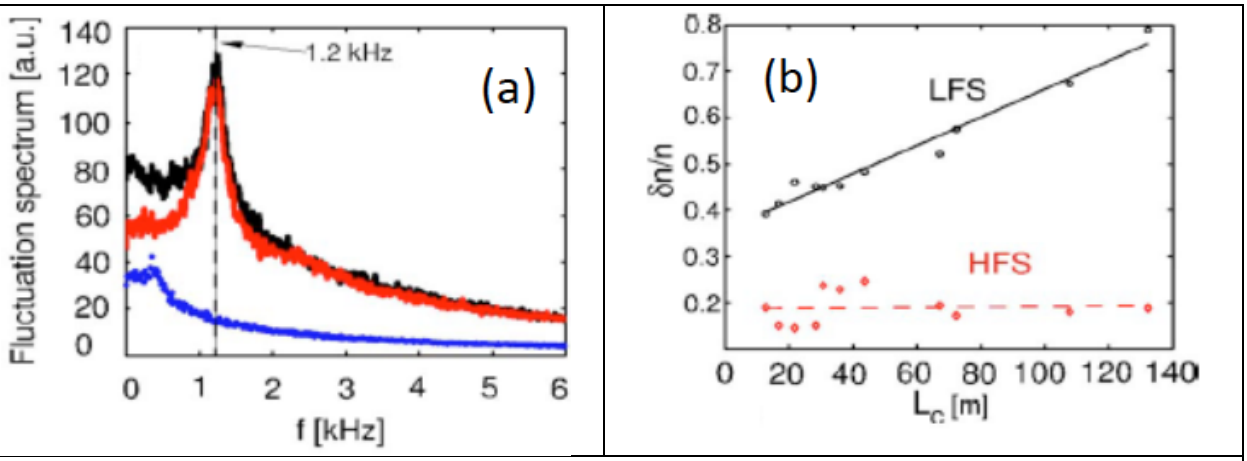

Fig. VII.7. (a) Fluctuation frequency spectra at HFS (of resistive drift wave, blue curve) and LFS (of resistive interchange mode, red and black curves) of the Helimak device; and (b) Relative density fluctuation at both LFS and HFS versus the connection length along helical magnetic field between the end-plates. Reproduced with permission from [22], © AIP Publishing 2006.

VII.2.7 Electromagnetic effects

As we can notice, all plasma waves we have considered so far were accompanied by electric currents. These currents generate fluctuating electromagnetic fields, which in plasma are manifested as the Alfven's waves. However, we neglected the electromagnetic effects in all preceding considerations. This can be justified for the case where the characteristic frequencies of the waves considered are much lower than the frequency of the Alfven waves or, to be more

precise, the frequency of the shear Alfven wave, $k_{||}V_A$, where $V_A = B/\sqrt{4\pi Mn}$ is the Alfven speed.

As an example, we consider the impact of electromagnetic effects on the collisionless drift wave described by Eq. (VII.14). Recall that to avoid the Landau damping on electrons, deriving Eq. (VII.14) we assumed $\omega < k_{||}V_{Te}$. Therefore, the inequality $\omega < k_{||}V_A$ is "automatically" satisfied for the case where $V_{Te} < V_A$ ($\beta_e \equiv nT_e/(B^2/4\pi) < m/M$), which gives $\omega < k_{||}V_{Te} < k_{||}V_A$. However, for larger β_e ($\beta_e > m/M$), the impact of electromagnetic effects can be important. To address this issue, in addition to the electrostatic potential φ we introduce a vector potential $\vec{A} = \vec{e}_z A_{||}(\vec{r},t)$ and will assume that both of them are small. Adopting the eikonal approximation for the perturbed quantities, we find the following contribution from the electromagnetic term to the amplitudes of fluctuating electric and magnetic fields: $\tilde{\vec{E}} = i\omega\vec{e}_z\tilde{A}_{||}/c$ and $\tilde{\vec{B}} = i\left(\vec{k}\times\vec{e}_z\right)\tilde{A}_{||}$. In addition, we have the following expression for the fluctuating electric current associated with the vector potential

$$\tilde{\vec{J}}_{||} = \frac{c}{4\pi}\left(\nabla\times\tilde{\vec{B}}\right) = \frac{ck_\perp^2}{4\pi}\tilde{A}_{||}\vec{e}_z. \qquad \text{(VII.68)}$$

The component of the fluctuating electric current perpendicular to $\vec{B}$ is described by Eq. (VII.55). As a result, using expressions (VII.55, VII.68), from the condition $\nabla\cdot\tilde{\vec{J}} = 0$ we find the relation between $\tilde{\varphi}$ and $\tilde{A}_{||}$:

$$\omega\tilde{A}_{||}/k_{||}c = \left(\omega/k_{||}V_A\right)^2\tilde{\varphi}. \qquad \text{(VII.69)}$$

For $\omega < k_{||}V_{Te}$, the electron density perturbation can be found from the stationary parallel electron momentum balance equation where electron temperature can be assumed constant. However, now we need to allow for small bending of the magnetic field lines, which is caused by electromagnetic effects. As a result, we have

$$-\frac{T_e}{e}k_{||}\frac{\tilde{n}_e}{n_0} + \left(\frac{\omega_*}{\omega} - 1\right)\frac{\omega\tilde{A}_{||}}{c} + k_{||}\tilde{\varphi} = 0. \qquad \text{(VII.70)}$$

Then, using Eq. (VII.69, VII.70), taking the ion density perturbation from Eq. (VII.11) and assuming the quasi-neutrality condition, we arrive at the following dispersion equation

$$\left(\omega_*/\omega - 1\right)\left\{1 - \left(\omega/k_{||}V_A\right)^2\right\} - \rho_s^2k_\perp^2 = 0. \qquad \text{(VII.71)}$$

Eq. (VII.71) describes the so-called drift-Alfven wave. In particular, for the large and small values of the $\omega_*/k_{||}V_A$ ratio it gives, respectively, the drift wave (Eq. (VII.14)) and the shear Alfven wave:

$$\begin{cases} \omega = \omega_*/(1+\rho_s^2k_\perp^2), & \text{for} \quad \omega_*/k_{||}V_A << 1 \\ \omega^2 = (k_{||}V_A)^2(1+\rho_s^2k_\perp^2), & \text{for} \quad \omega_*/k_{||}V_A >> 1 \end{cases}. \qquad \text{(VII.72)}$$

We notice that in our evaluation of electromagnetic effects we assumed so far that the magnetic field is constant and straight, $\vec{B} = B\vec{e}_z$. As a result, the non-divergence-free cross-field

plasma current still appears only due to ion inertia, recall Eq. (VII.55). However, in a tokamak magnetic configuration, we should allow for the contribution of the diamagnetic current (VII.54). Considering low β plasma and being interested in the waves with the characteristic frequency $\omega \tilde{>} k_{||} V_A$, using Eq. (VII.12) for ion density perturbation we can neglect the ion dynamics along the magnetic field lines (which gives a contribution $\sim \beta << 1$). Then, from the vorticity equation (VII.56) and the electron parallel momentum balance equation (VII.64), keeping in mind the relation (VII.68) and the plasma quasi-neutrality condition, after some algebra, we come to the following dispersion equation

$$\left(1-\omega_*/\omega\right)\left\{\omega^2+\gamma_I^2\left(1-\rho_s^2k_\perp^2(\omega_*/\omega)\right)-(k_{||}V_A)^2\right\}-\rho_s^2k_\perp^2(k_{||}V_A)^2=0\,. \qquad \text{(VII.73)}$$

For $\rho_s^2 k_\perp^2 << 1$, Eq. (VII.73) is reduced to

$$\left(1-\omega_*/\omega\right)\left(\omega^2+\gamma_I^2-(k_{||}V_A)^2\right)=0\,, \qquad \text{(VII.74)}$$

which describes the drift wave, $\omega=\omega_*$, and a proxy for the ideal ballooning mode [37] with

$$\omega^2=-\gamma_I^2+(k_{||}V_A)^2\,. \qquad \text{(VII.75)}$$

We notice that for simplicity, we considered the case where only plasma density has a cross-field gradient, whereas electron temperature was assumed to be constant and the ions were "cold". However, as we discussed, the mechanism of the interchange mode is related to the polarization of plasma protrusion due to the magnetic drifts (recall Fig. VII.2), which, according to Eq. (VII.54), is determined by the total plasma pressure. As a result, a more complete consideration shows that instead of the expression (VII.59), γ_I should be defined, assuming $k_y^2/k_\perp^2 \approx 1$, as

$$\gamma_I^2 \equiv \frac{2}{MnR}\frac{d\ell n(P_{tot})}{dx}\,, \qquad \text{(VII.76)}$$

where P_{tot} is the total equilibrium plasma pressure. Then Eq. (VII.69) shows that for the "bad" curvature case, $dP_{tot}/dx<0$, and large parallel wavelength, the magnetic drift of the charged particles can destabilize plasma perturbations. Estimating $k_{||}\sim 1/qR$, where q is the safety factor, from Eq. (VII.75, VII.76) we find that the instability starts for the so-called "MHD ballooning parameter" α exceeding unity:

$$\alpha \equiv q^2 R\frac{d\beta}{dx}>1\,. \qquad \text{(VII.77)}$$

The eigenfunction of the perturbed plasma pressure for the ballooning mode in ITER, found from the numerical simulation in [38], is shown in Fig. VII.8.

VII.2.8 Effect of "open" magnetic field lines

Here we consider how a contact of the plasma with material surfaces (e.g. limiters, divertor targets) in the SOL region can affect plasma stability. As we found, plasma instabilities, this way or another, result in a fluctuating electric current along the magnetic field lines. The volumetric resistive effects associated with this current can cause dissipative plasma instabilities (e.g. recall Eq. (VII.32)). However, in Ch. IV it was shown that the plasma current into a material surface (which we will, for simplicity, assume perfectly conducting) is related to some variation of the electrostatic potential through the sheath, φ_{sh}, bridging the material surface and the plasma.

Then the expression for the low magnitude of electric current perturbation to the target, $\tilde{J}_{\parallel}^{tar}$, can be found by linearizing the expression (IV.18), which, ignoring electron emission from the surface and assuming a normal incidence of the magnetic field onto the target, gives (see also [39], [40]):

$$\tilde{J}_{\parallel}^{tar} = en_{sh}C_s(T_e)\left\{\frac{e\tilde{\varphi}_{sh}}{T_e} - \left(\frac{1}{2}+\Lambda_{sh}\right)\frac{(\tilde{T}_e)_{sh}}{T_e}\right\} + \left(\frac{\tilde{n}_{sh}}{n_{sh}} + \frac{1}{2}\frac{(\tilde{T}_e)_{sh}}{T_e}\right)J_{\parallel}^{tar}, \quad \text{(VII.78)}$$

where $\Lambda_{sh} = e\varphi_{sh}/T_e$.

The "boundary" condition Eq. (VII.78) can result in a new type of instability and alter some modes we have considered so far. First, we consider an impact of this boundary condition on the interchange mode described by Eq. (VII.59, VII.60). For simplicity, we analyze the SOL plasma at the outer side of the torus for a double null magnetic configuration (see Fig. I.6a). We take the cold ion approximation and assume that the background electron temperature is homogeneous and rather high so that the plasma can be considered collisionless. For such a case, both the electrostatic potential and plasma density are virtually constant along the magnetic field lines. We will also ignore the toroidality-induced compressibility effects and take $\tilde{T}_e = 0$. Finally, we consider the case with no unperturbed plasma current to the material surface. As a result, from Eq. (VII.78) we have

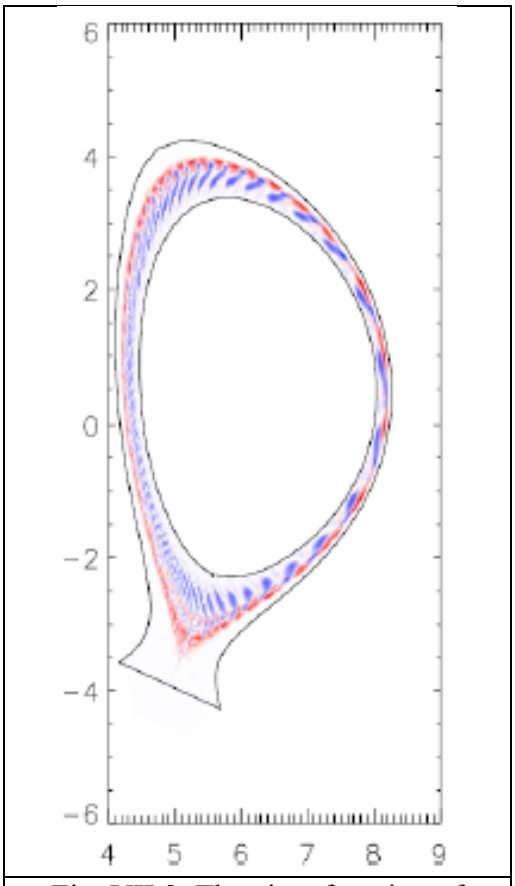

Fig. VII.8. The eigenfunction of perturbed plasma pressure for the ballooning mode in ITER. Reproduced with permission from [38], © IAEA 2011.

$$\tilde{J}_{\parallel}^{surf} = en_{sh}C_s(T_e)\frac{e\tilde{\varphi}_{sh}}{T_e}. \quad \text{(VII.79)}$$

Then, integrating Eq. (VII.56) along the magnetic field lines and approximating them as straight lines along the major tokamak axis, using Eq. (VII.5) for the density evolution and the boundary condition (VII.79), we find [41]

$$\omega + \frac{\gamma_I^2}{\omega} + \frac{2i}{\rho_s^2 k_\perp^2}\frac{C_s}{L_{cl}} = 0. \quad \text{(VII.80)}$$

Here L_{cl} is the "connection length" – the length between the divertor plates along the magnetic field line. Comparing Eq. (VII.60) and (VII.80) we see that the boundary condition (VII.79) plays the role of effective "sheath resistivity", which exceeds the volumetric resistivity caused by the Coulomb collisions for

$$\frac{\lambda_{Ce}}{L_{cl}} \gtrsim \sqrt{\frac{m}{M}}. \quad \text{(VII.81)}$$

Apart from the modification of existing instabilities, the boundary condition (VII.78) can result in a new type of instability. In particular, it appears that the interplay of the radial gradient of electron temperature in the SOL and the sheath boundary conditions can drive instability that is not related to the interchange drive considered in Eq. (VII.80) [42]. The reason for such instability is the phase shift between the volumetric and surface dynamics of the electrostatic potential. To demonstrate the underlying physics of this instability, we take the cold ion approximation, assume that the background plasma density is homogeneous and the electron temperature is rather high so that the plasma can be considered collisionless and the electrostatic potential and electron temperature along the magnetic field lines are virtually constant. Then, integrating Eq. (VII.56) along the magnetic field lines (approximating them as straight lines along the major tokamak axis) and ignoring toroidality effects we find

$$-i\omega\rho_s^2 k_\perp^2 \frac{e\tilde{\varphi}}{T_e} + 2\frac{C_s}{L_{cl}}\left\{\frac{e\tilde{\varphi}}{T_e} - \left(\frac{1}{2} + \Lambda_{sh}\right)\frac{\tilde{T}_e}{T_e}\right\} = 0 . \qquad \text{(VII.82)}$$

Finding the electron temperature perturbation $\tilde{T}_e$ from the equation similar to Eq. (VII.36), we find the following dispersion equation

$$\omega + \frac{2i}{\rho_s^2 k_\perp^2}\frac{C_s}{L_{cl}}\left\{1 - \left(\frac{1}{2} + \Lambda_{sh}\right)\frac{\omega_{*,e}}{\omega}\right\} = 0 , \qquad \text{(VII.83)}$$

where

$$\omega_{*,e} = -\frac{cT_e}{eB_0}\frac{d\ell n(T_e)}{dx}k_y . \qquad \text{(VII.84)}$$

One can see that the growth rate of the instability described by Eq. (VII.83) can be of the order of $\omega_{*,e}$.

So far we consider the plasma waves and instabilities related to plasma polarization caused by the electron dynamics along the magnetic field and the cross-field magnetic drift of the charged particles. However, plasma polarization can also be related to the interplay of the electric current along the magnetic field lines and cross-field inhomogeneity of the plasma conductivity (e.g. see [43], [Furth63]). Indeed, for the case where the plasma current flows only along the magnetic field lines, it should be maintained constant. However, displacement of some plasma slab inclined to the magnetic field lines, similar to that shown in Fig. (VII.9), causes a perturbation of the plasma conductivity along the magnetic field lines. Therefore, to keep the electric current constant, some additional electric field appears inside the slab, caused by charge accumulation at the boundaries of the slab. But due to the inclination of the slab, a cross-field electric field and corresponding $\vec{E}\times\vec{B}$ plasma drift emerge, which can displace this fluid element even more.

Indeed, from the conservation of parallel current, $j = \sigma(x)E = \text{const.}$, where $\sigma(x)$ is the plasma conductivity and E is the electric field, we find

$$E\frac{d\sigma(x)}{dx}\tilde{x} + ik_z\sigma\tilde{\varphi} = 0 . \qquad \text{(VII.85)}$$

Here $\tilde{x}$ is the displacement and $\tilde{\varphi}$ the perturbation of the electrostatic potential. However, on the other hand, we have

$$V_x \equiv \frac{d\tilde{x}}{dt} = -\frac{c}{B_0}\nabla\tilde{\varphi}\times\vec{e}_z . \qquad \text{(VII.86)}$$

As a result, from Eq. (VII.85, VII.86) we find

$$\frac{d\tilde{x}}{dt} = \frac{k_y}{k_z}\frac{cE}{B_0}\frac{d\ell n(\sigma)}{dx}\tilde{x}\,, \qquad \text{(VII.87)}$$

and for the proper sign of the k_y / k_z ratio (which defines the inclination angle of the slab with respect to the direction of the magnetic field), we have the so-called current-convective instability with a characteristic growth rate

$$\gamma = \left|\frac{cE}{B_0}\frac{d\ell n(\sigma)}{dx}\frac{k_y}{k_z}\right|. \qquad \text{(VII.88)}$$

We should recall that the electric conductivity of plasma is $\sigma \propto T_e^{3/2}$, therefore the perturbation of conductivity, which drives the current-convective instability, is associated with inhomogeneity of the electron temperature along the magnetic field lines. However, electron temperature perturbations along the magnetic field can be washed away by very fast parallel electron heat conduction, $\kappa_e \propto T_e^{5/2}$, and no instability will be possible. However, recently it was shown [44] that in asymmetric "detached divertor" regimes, where the plasma temperature in the inner divertor falls to ~eV range but the outer divertor is still relatively hot, $T_{hot} \sim 10\,\text{eV}$), current-convective instability can be very "active" and important in plasma transport in the inner divertor. There are two reasons for this: i) the electron thermal conductivity effects are suppressed in the inner divertor and ii) the asymmetry of the electron temperatures in the inner and outer divertors results in onset of a large electrostatic potential drop, $U \sim \text{few} \times T_{hot}$, through the inner divertor leg, which boosts the growth rate of the current-convective instability there, see Eq. (VII.88).

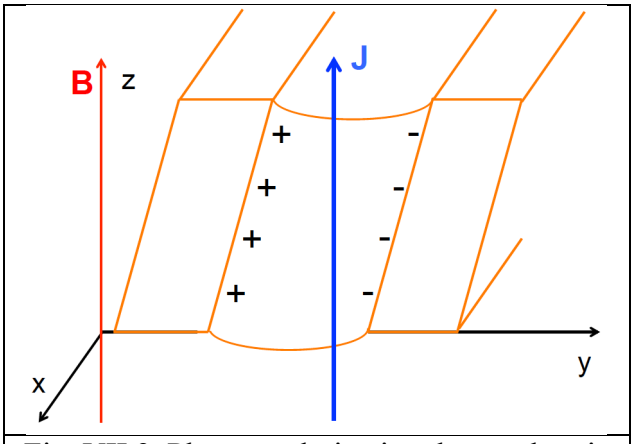

Fig. VII.9. Plasma polarization due to electric current along the magnetic field and cross-field inhomogeneity of plasma conductivity.

VII.2.9 Impact of magnetic shear

So far, considering the slab approximation of a magnetic confinement device, we assumed that all magnetic field lines are parallel to each other. However, in practice, this is not the case and the direction of the vector $\vec{b} = \vec{B}/B$ rotates around the minor radius $\vec{r}$ with increasing r, similar to that shown for the slab geometry in Fig. VII.10a where the x-coordinate plays the role of the minor radius. Therefore, if we specify the poloidal (y-direction) component of the wavenumber (k_y), the effective parallel component of the wave vector will depend on the minor radius. One can see this from Fig. VII.10b, where the blue and orange stripes along the toroidal (z-coordinate) correspond to different phases of the perturbed plasma parameters with given k_y and the vector $\vec{b}$ is shown for different radial (x-coordinate) locations.

In simplified analytic consideration of the magnetic shear effects, the following model for the magnetic field it is often used:

$$\vec{B} = B\left(\vec{e}_z + \vec{e}_y \frac{x}{L_s}\right), \qquad \text{(VII.89)}$$

where L_s determines the "strength" of the magnetic shear and the second term describes the "rotation" of the direction of the magnetic field lines with varying "radial" coordinate.

As a result of the magnetic shear, the wavenumber $k_\parallel$ along the magnetic field lines varies within the eigenfunction of a particular mode of the wave packet. Therefore, growth of the waves, the dispersion of which depends strongly on the magnitude of $k_\parallel$ (e.g. the drift waves, recall Eq. (VII.15, VII.28)), can be significantly restricted (e.g. see [45], [46], [47], [48], and the references therein). In addition, the magnetic shear can also shrink the radial extent of the mode eigenfunction, which can imply the reduction of the contribution of this mode to anomalous transport (e.g. see [28], [49], [50], and the references therein).

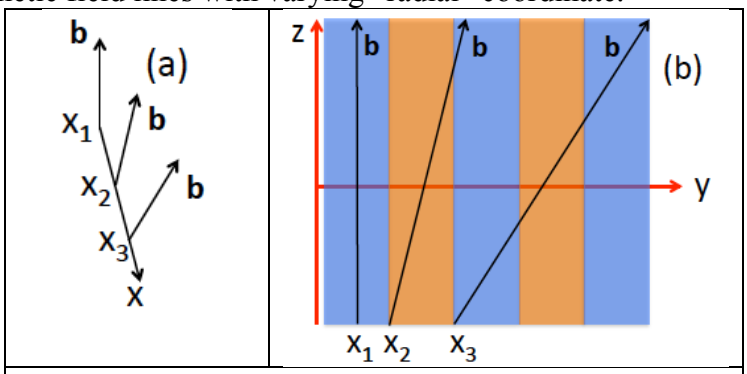

Fig. VII.10. Schematic view of the variation of the vector $\vec{b}$ (a) and effective $k_\parallel$ (b) along "radial" direction x.

As an example, in Fig. VII.11 one can see that the increasing magnetic shear (decreasing L_s) results in the reduction of the relative amplitude of plasma density fluctuations caused by the excitation of collisionless drift waves.

However, the simple model of the magnetic field (VII.83) can more or less adequately describe the effect of the magnetic shear for the case where the shear is not varying much on a magnetic flux surface. This is not the case for the magnetic flux surfaces close to the separatrix which contains at least one X-point where the magnitude of the poloidal magnetic field, B_p, is zero. In the vicinity of the X-point, the magnitude of the poloidal magnetic field is proportional to the distance from the X-point, ℓ_X (for the case of the first-order X-point), so $B_p(\ell_X) \propto \ell_X$. We notice that the similarity of such dependence of $B_p(\ell_X)$ with the model (VII.89) is illusory. The z-direction in Eq. (VII.83) is the direction of the total magnetic field at some effective "magnetic flux surface" corresponding to $x = 0$, whereas for the case of the magnetic field in the vicinity of the X-point, we are dealing with the "exact" poloidal and toroidal magnetic fields.

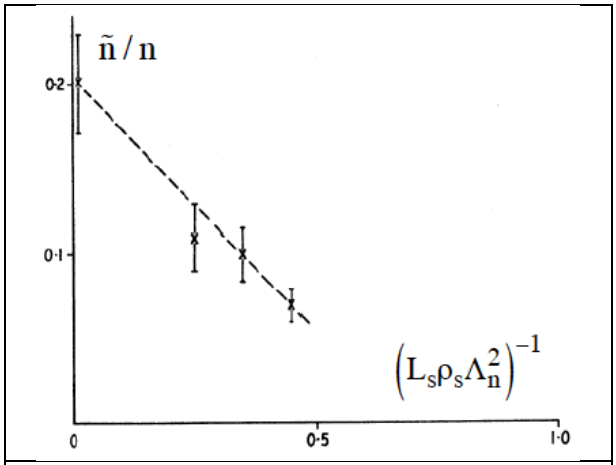

Fig. VII.11. Magnetic shear suppression of plasma density fluctuations, caused by the excitation of collisionless drift waves. Reproduced with permission from [46], © American Physical Society 1970.

Such a structure of the magnetic field near the X-point results in a very strong magnetic shear localized there. One can see this by considering how the poloidal projection of a magnetic flux tube cross-section evolves along the tube, Fig. VII.12. The magnetic flux in the tube is mainly determined by the large toroidal magnetic field that does not vary much, so we can consider the area of the poloidal cross-section of the tube to be almost constant if the pitch angle of the magnetic field line $B_p / B << 1$, which is always the case near the X-point. Assume that the magnetic flux tube has a circular poloidal cross-section closer to the mid-plane (see the contour (1) in Fig. VII.12). The shape of this cross-section evolves along the tube, becoming a thin oval close to the X-point (contours 2 and 3) since the magnetic surfaces that determine the radial extent of the cross-section diverge there. The variation of the poloidal width of the tube cross-section, $\delta\ell_p$, can be estimated taking into account that $B_p(\ell_X) \propto \ell_X$ [51]:

$$\frac{\delta\ell_p}{\delta\ell_p(0)} \approx \frac{\ell_X}{\ell_X(0)}. \qquad \text{(VII.90)}$$

where $\ell_X(0)$ and ℓ_X are the initial and current distances from the X-point, $\ell_X(0) >> \ell_X$ (the position 0 corresponds to the location farther from the X-point. So for the magnetic flux coming close to the X-point, we have $\delta\ell_p << \delta\ell_p(0)$.

In practice, the effect of "poloidal compression" of the flux tubes can be so strong that even flux tubes originated in the midplane at a distance ~centimeter from the separatrix and having a ~centimeter cross-field radius, are squeezed poloidally to the scale below the ion gyro-radius in the vicinity of the X-point [51]. Similarly, any wavy structure originated at the midplane and having a long wavelength parallel to the magnetic field will experience a strong reduction of the effective poloidal wavelength in the vicinity of the X-point, which will result in strong dissipation effects and effectively stop the wave penetration through the X-point region from the midplane into the divertor region and vice versa [51], [52] [53]. Therefore, turbulent processes in the divertor region and SOL become disconnected. However, strong dissipative effects near the X-point can play a role somewhat similar to volumetric dissipation and result in a new type of instabilities (e.g. see [54], [55] and the references therein).

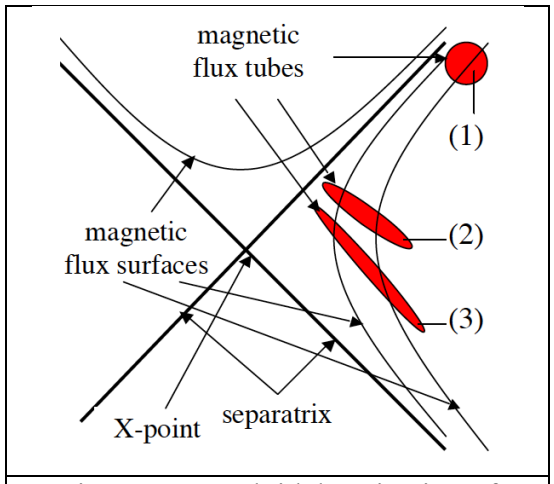

Fig. VII.12. Poloidal projection of magnetic flux tube, having circular cross-section at the "mid-plane", in different toroidal locations.

The evidence of turbulence disconnection between the divertor region and SOL was found in the tokamak experiments [56], where no correlation between midplane and divertor fluctuations was observed for a rather high poloidal mode number. The poloidal correlation length found in these experiments (see Fig. VII.13) was in agreement with the mapping of the magnetic flux tubes. However, the perturbations with a low poloidal wavenumber at the outer midplane can "survive" the fierce squashing of the magnetic flux tube in the vicinity of the X-point and show a strong correlation between the fluctuation measurements in the midplane and in the divertor volume [57]. Further experimental details of the X-point effects on plasma turbulence can be found in [58], [59].

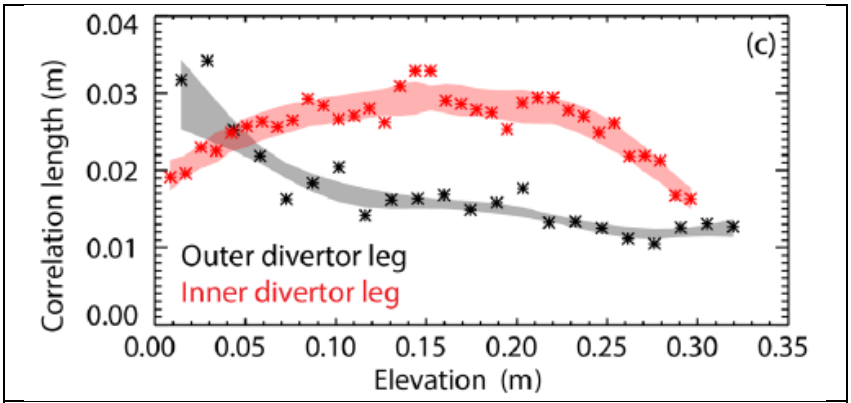

Fig. VII.13. Poloidal correlation length of blobs (coherent filamentary structures) in outer and inner divertor legs as the functions of the distance to divertor targets is in agreement with the mapping of the magnetic flux tubes. Reproduced with permission from [56], © IAEA 2018.

We notice that strong squeezing of the magnetic flux tube caused by the X-point effects poses a substantial challenge to both theoretical and numerical studies of these effects. First of all, for the case where the effective poloidal wavelength in the vicinity of the X-point becomes comparable to or even smaller than the ion gyro-radius ρ_i, neither fluid nor gyro-kinetic models of plasma dynamics become applicable, whereas full 3D3V (three-dimensional in both the coordinate and velocity space) kinetic description of plasma turbulence is not feasible. In addition, the small spatial scale that has to be resolved near the X-point brings another complication for numerical modeling of the X-point effects. As a result, the applicability and validity of modern numerical studies of the X-point effects on the edge plasma instabilities and, in particular, turbulence are somewhat questionable. In analytic theory, the X-point effects are often described with some effective boundary conditions for the "standard" differential equations for the edge plasma waves at the "entrance" to the X-point region (see [53], [54], [55], and the references therein). These boundary conditions assume that X-point dissipation results in a fast decrease of the electrostatic potential in the direction of the X-point, which is usually described as an evanescent wave. However, even in this case, the models used for such effective closures only cover extreme cases where the poloidal scale of the electrostatic potential in the wave is either still larger than ρ_i or much smaller than that.

VII.2.10 Impact of plasma "macro- and mesoscale" flows

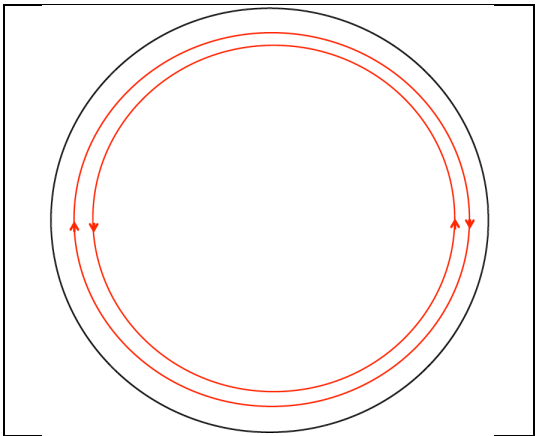

Fig. VII.14. Schematic view of a poloidal sheared flow of plasma (red lines) with a small radial scale length in a tokamak.

So far, we considered the waves and instabilities in plasma at rest. However, quite often some specific, macro- and mesoscale, plasma flows can develop. Such flows can emerge due to different nonlinear inherent processes associated with plasma turbulence or can be driven by outside effects such as, for example, injection of neutral beams used for plasma heating. In tokamaks, flows having very low effective poloidal wave numbers virtually do not contribute to anomalous cross-field plasma transport since such flows mostly have only poloidal and/or toroidal components of the plasma velocity. However, the characteristic radial scale length of such flows can be rather small (see Fig. VII.14). As a result, the poloidal component of the plasma flow velocity may have a large radial shear, V_0', which can drastically

modify both development of the plasma instabilities and anomalous plasma transport (e.g. see Refs. [60], [4] and the references therein).

Although both poloidal and toroidal flows can be important, here, for simplicity, we will discuss mostly pure poloidal plasma flows driven by the radial electric field.

Very often an impact of the velocity shear is illustrated as continuous stretching in time of plasma turbulent eddies – the contours of equipotential $\varphi(\vec{r},t)$, see Fig. VII.15.

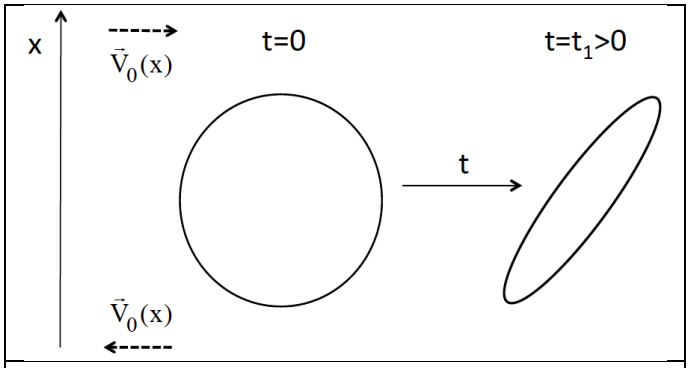

Fig. VII.15. Stretching of turbulent eddy caused by the plasma velocity shear.

It is also often presumed that the plasma instability is quenched when $|V_0'|$ becomes larger than the growth rate of the instability, γ_{inst}, in the absence of the velocity shear (e.g. see [61], [4]). However, in practice, the situation is more complex and in general case, the velocity shear can even increase the growth rate of plasma instability.

Just for an illustration we consider the Rayleigh-Taylor instability of a stratified fluid in a gravity field and take into account the impact of the velocity shear (e.g. see [27], [62], [63] [64], [65], [67] and the references therein). Recall that the Rayleigh-Taylor instability can be considered as a proxy for the interchange plasma instability. We take the unperturbed fluid velocity as $\vec{V}_0(\vec{r}) = V_0(x)\vec{e}_y$ and assume that gravitational acceleration is in the x-direction. Then, in the Boussinesq approximation, small perturbations of the fluid velocity stream function $\tilde{\psi}(x,y,t)$ are described by the following partial differential equation

$$\hat{L}_{RT\&V'}(\tilde{\psi}) = \hat{\Omega}\left\{\hat{\Omega}\nabla^2\tilde{\psi} - \frac{\partial\tilde{\psi}}{\partial y}\frac{d^2V_0}{dx^2}\right\} + \frac{1}{\rho}\frac{d\rho}{dx}\frac{\partial^2\tilde{\psi}}{\partial y^2} = 0, \qquad \text{(VII.91)}$$

where $\hat{L}_{RT\&V'}(...)$ is an operator describing the linear phase of the evolution of the stratified fluid velocity perturbation in the presence of gravity and unperturbed horizontal fluid flow, and $\hat{\Omega}(...) \equiv \partial(...)/\partial t - V_0(x)\partial(...)/\partial y$. Looking for the solution of Eq. (VII.91) in the form of a combination of the eigenfunctions, $\tilde{\psi}(x,y,t) = \tilde{\psi}(x)\exp(-i\omega t + ik_y y)$, from Eq. (VII.91) we arrive at the following generalized version of Eq. (VII.61):

$$\frac{d^2\tilde{\psi}}{dx^2} - k_y^2\tilde{\psi} + \frac{1}{\rho}\frac{d\rho}{dx}\frac{gk_y^2}{\tilde{\omega}^2}\tilde{\psi} - \frac{d^2\tilde{\omega}}{dx^2}\frac{\tilde{\psi}}{\tilde{\omega}} = 0, \qquad \text{(VII.92)}$$

where $\tilde{\omega} = \omega - k_y V_0(x)$. This equation is usually solved as an eigenfunction-eigenvalue problem, where the role of the eigenvalues goes to ω. We notice that the last term in Eq. (VII.92) can drive the Kelvin-Helmholtz [27] and facilitate the Rayleigh-Taylor [67] instabilities.

Assuming that in the fluid at rest, the Rayleigh-Taylor instability develops, the impact of the velocity shear can be characterized by the effective Richardson number which in our case we define as $Ri = g\,|d\ell n(\rho)/dx|\,(V_0')^{-2}$. The case where a stratified fluid is bounded by two

horizontal walls separated by a distance h was considered in [62] in the Boussinesq approximation.

It was assumed that $d\ell n(\rho)/dx$ and V_0' are constants and zero perturbed fluid velocity at the walls was used as the boundary conditions. It was shown that for such settings, no unstable eigenfunction-eigenvalue solutions of Eq. (VII.92) exist for $Ri < Ri_{crit} \approx 1 \div 2$, where Ri_{crit} depends on $|k_y|h$ and stabilization of smaller k_y requires a somewhat lower Ri_{crit}. Thus, these findings are consistent with the simplified physical picture of the impact of shear stabilization on the instability described by the inequality $|V_0'| \gtrsim \gamma_{inst}$. However, the results of the numerical solution of Eq. (VII.92), shown in Fig. VII.16, for the case of the density profile given by Eq. (VII.63), constant V_0', and the $m = 0$ mode, portray a different picture.

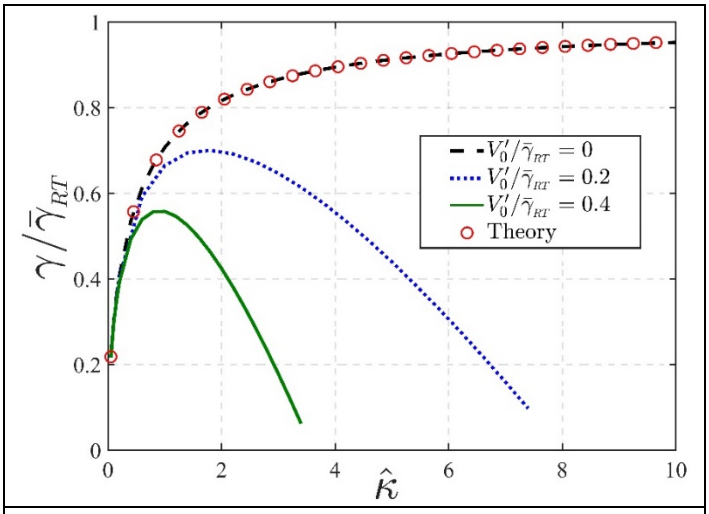

Fig. VII.16. Impact of V_0' on the growth rate of the Rayleigh-Taylor instability for different $\hat{\kappa} = |k_y| w$ found numerically for the density profile given by Eq. (VII.63). Reproduced with permission from [66], © AIP Publishing 2020.

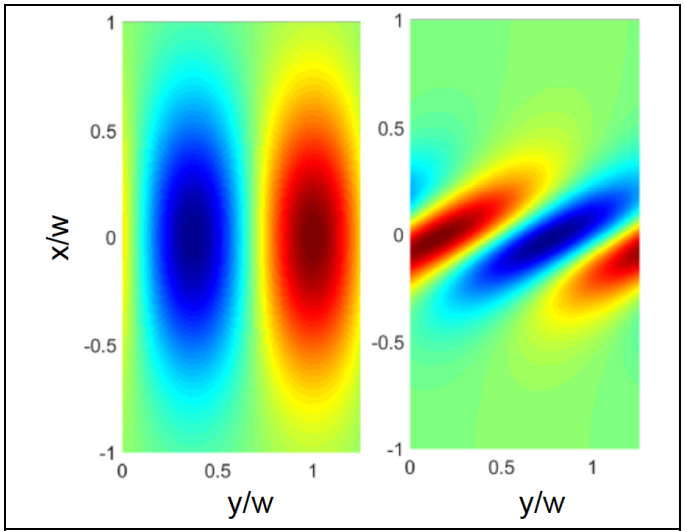

Fig. VII.17. Impact of the velocity shear on the eddies corresponding to the eigenfunction found from numerical simulation of Eq. (VII.92) for $\hat{\kappa} = 2$ and $Ri_0^{-1} = 0$ (left) and $Ri_0^{-1} = 6.25$ (right). Reproduced with permission from [66], © AIP Publishing 2020.

They demonstrate that for $|k_y| w > 1$, where $\gamma_{RT_{m=0}} \approx \bar{\gamma}_{RT}$, stabilization occurs at $Ri_0 \equiv (\bar{\gamma}_{RT}/V_0')^2 > 1$, whereas for small $|k_y| w$ unstable solutions of Eq. (VII.92) persist even though in this case $\gamma_{RT_{m=0}} < |V_0'|$ [66]. Similar results were obtained in Ref. [67] for a density profile somewhat different from (VII.63). The same trend of the impact of the poloidal velocity shear on the growth rate of the resistive interchange modes was found in [69], [68].

Such resilience of the Rayleigh-Taylor and interchange instabilities to velocity shear stabilization at small $|k_y| w$ can be understood from the following consideration. We notice that the case of $|k_y| w \to 0$ corresponds to the

eigenfunction that extends along the x-coordinate to the distance $\sim|k_y|^{-1}$ (see Eq. (VII.64)) which is much larger than the width of the density "step" w in Eq. (VII.63).

Therefore, the mode does not "feel" the details of the density variation, but only the size of the density "step". Thus, the case of $|k_y|\,w \to 0$ can be considered by adopting the exact step-function of the density profile, $\rho(x) = \bar{\rho} - \Delta\rho\{\theta(x) - 1/2\}$, where $\theta(x)$ is the Heaviside function: $\theta(x<0) = 0$, $\theta(x>0) = 1$. Then, from Eq. (VII.92) we have $\tilde{\psi}(|x| > 0) = \exp(-|k_y x|)$ and integrating Eq. (VII.92) around $x = 0$, we find that the growth rate is $\gamma^2_{RT_{m=0}} = \bar{\gamma}^2_{RT}\,|k_y|\,w$ and the velocity shear does not change it. The eddies corresponding to the eigenfunctions found from the numerical solution of Eq. (VII.92) are shown in Fig. VII.17. As one can see, in accordance with some expectations (recall Fig. VII.15), the velocity shear indeed causes some stretching of the eddies. We notice that at large velocity shear, $|V_0'|\,\hat{\kappa} > 1$, the localized solution of the RT instability cease to exist (see [66] for details).

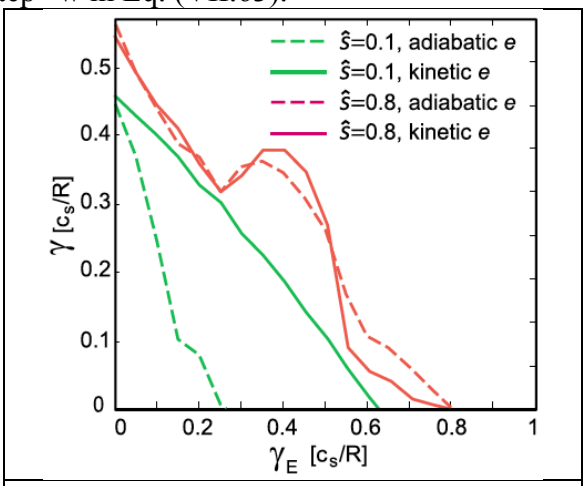

Fig. VII.18. The growth rate of the ITG instability versus plasma flow shear rate $\gamma_E \propto V_0'$ for different values of magnetic shear $\hat{s}$. Reproduced with permission from [77], © AIP Publishing 2012.

However, we should keep in mind that even though we use a slab model of the Rayleigh-Taylor as a proxy for the curvature-driven instabilities in a tokamak, in practice this model does not allow for many important effects including both the poloidal and toroidal periodicities of the tokamak geometry, the centrifugal and Coriolis forces, electromagnetic and other effects. As a result, theoretical assessment of the role of the plasma flows, both poloidal and toroidal, on different instabilities becomes more complex (e.g. see [70], [71], [72], [73], [74], [75], [76], [77] and the references therein).

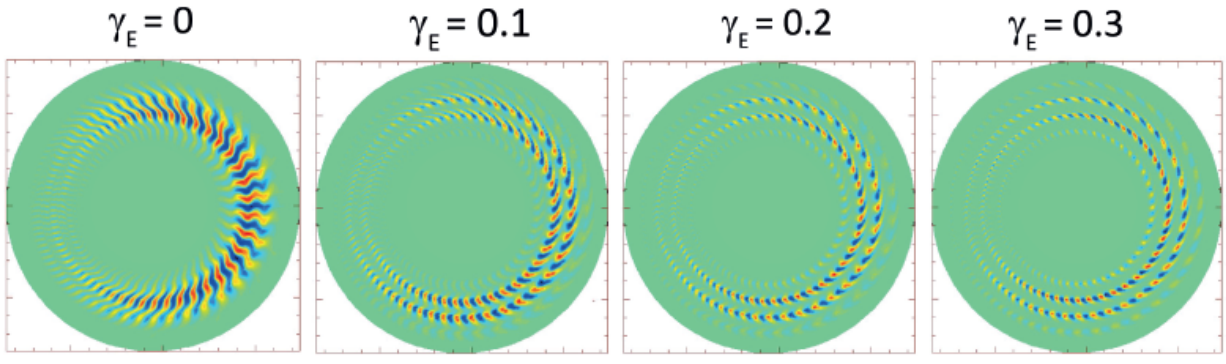

Fig. VII.19. Eigenfunctions of the electrostatic potential of toroidal ITG modes in a tokamak with increasing shear of the plasma flow, $\gamma_E \propto V_0'$, [78]. V. I. Dagnelie, private communication, 2020.

Nonetheless, it appears that the plasma flow shear is very efficient in reducing the growth rate of some plasma instabilities related to the impact of effective "gravity" associated with the magnetic drifts (e.g. see Fig. VII. 18).

In addition to the impact on the growth rate of the instabilities, both the poloidal and toroidal velocity shear can significantly alter the eigenfunctions of the modes (see Fig. VII.19, VII.20), which also affects anomalous transport of plasma.

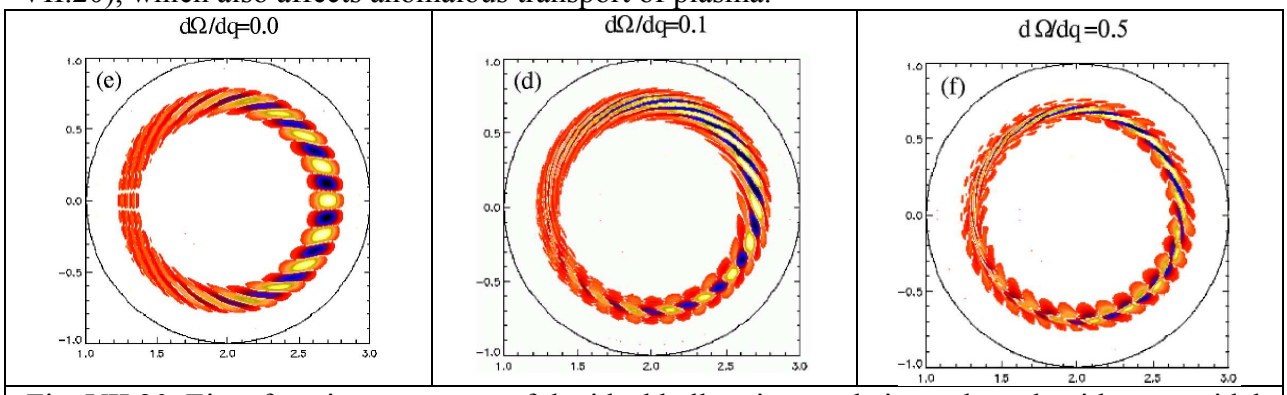

Fig. VII.20. Eigenfunctions structure of the ideal ballooning mode in a tokamak with no toroidal velocity shear (eft); medium shear $d\Omega/dq$ (middle) and high shear (right), were Ω and q are the toroidal angular velocity of the plasma and the safety factor. Reproduced with permission from [74], © American Physical Society 2004.

However, we should notice that many studies of linear plasma instabilities rely on treating the corresponding partial differential equations, which describe different instabilities, as the eigenfunction-eigenvalue problems (e.g. recall our derivation of the expressions (VII.20) and (VII.64)). Yet, the general solution of these differential equations can be represented as a combination of eigenmodes only for the case where the operators defining these equations are Hermitian. And this is usually not the case when the unperturbed flow velocity is included. For example, the operator $\hat{L}_{RT\&V'}(...)$ is not Hermitian for a finite fluid velocity. As a result, in the non-Hermitian case, the combination of the eigenmodes (even if they exist) cannot describe the entire linear evolution of fluid parameter perturbations (e.g. see [79], [80] and the references therein). In some, although rather limited cases (in particular, constant velocity shear), this issue can be overcome in analytic or quasi-analytic considerations by implying the so-called non-modal approach, where after some transformation of the variables, including usage of the variable $\zeta = y - V'_0 xt$ describing effective squashing of a fluid element by the sheared flow, the problem of interest can be solved as an initial value problem. Usually the perturbations described by non-modal approach could increase with time only as t^p, where p is some constant. Therefore they become important for the case where the localized modes either stable or cease to exist. For further discussion of this approach see [81], [79], [65], [82] and the references therein.

Whereas the "rule of thumb" of velocity shear stabilization, $|V'_0| \gtrsim \gamma_{inst}$, works, in a ballpark, for the plasma instabilities related to effective "gravity" associated with the magnetic drifts (e.g. toroidal ITG, ballooning instability), it appears that the shear of poloidal plasma velocity makes a very mild impact on the resistive drift wave instability. By adding a poloidal plasma flow with a constant velocity shear, so that $\tilde{\omega}(x) = \omega - V'_0 k_y x$, from Eq. (VII.12), (VII.31), assuming that $\tilde{\phi}(x,y,t) = \tilde{\phi}(x)\exp(-i\omega t + ik_y y)$, in the Boussinesq approximation and

for the plasma density profile (VII.18), which gives $\omega_*(x) = \hat{\omega}_* \cosh^{-2}(x/w)$, we obtain the following equation

$$\rho_s^2 \frac{d^2\tilde{\phi}}{dx^2} - \left(1 + k_y^2\rho_s^2 - \frac{\omega_*(x)}{\tilde{\omega}(x)} + i\frac{\tilde{\omega}(x) - \omega_*(x)}{\nu_{||}}\right)\tilde{\phi} = 0, \qquad \text{(VII.93)}$$

where for simplicity we omit the unimportant here parallel electron heat conduction and thermal force effects.

Some particular results found from the numerical solution of Eq. (VII.93), which show the impact of V_0' on the growth rate, are demonstrated in Fig. VII.21. As one can see, unlike the Rayleigh-Taylor instability (recall Fig. VII.16), there is a very mild impact of V_0' on the growth rate of the dissipative drift wave instability, even though $|V_0'| >> \gamma_{inst}$. However, similar to the RT mode, at relatively large velocity shear, $|V_0'| > |V_0'|_{loc}$, no localized solution of the resistive drift wave was found [66]. All of these observations have a rather simple explanation.

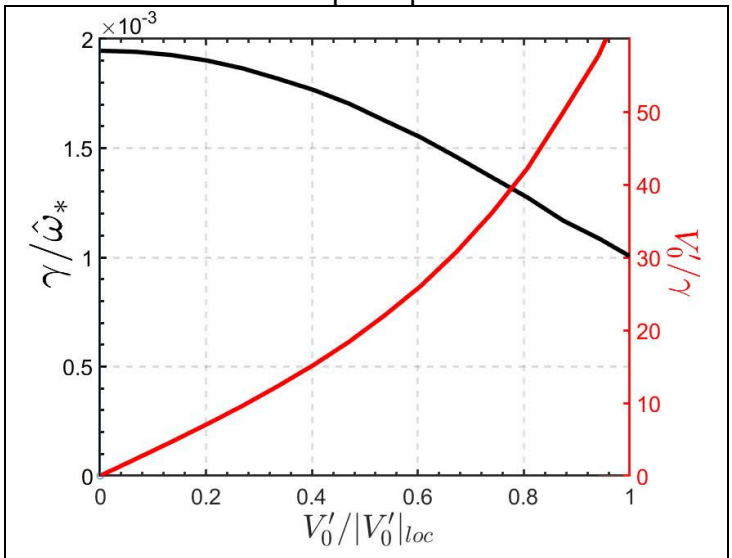

Fig. VII. 21. Growth rate and the V_0'/γ ratio of the dissipative drift wave instability found from the numerical solution of Eq. (VII.93), as a function of V_0'. Other parameters used in these simulations are: $k_y\rho_s = 0.5$, $w/\rho_s = 30$, and $\nu_{||}/\hat{\omega}_* = 50$.

First, we discuss the key difference between the RT/interchange modes and drift waves. The Rayleigh-Taylor instability is associated with the dynamics of density protrusions, which can be directly altered by the sheared flow. Similarly, the interchange plasma instability is associated with the dynamics of plasma density perturbations with embedded electric charges originated from almost "irreversible" cross-field magnetic drift effects. Spatial distribution of these charges produces $\vec{E}\times\vec{B}$ drifts, which, finally, drive the instability. Similar processes are relevant to all plasma instabilities driven by magnetic drift effects (e.g. the toroidal ITG and ballooning modes). Therefore, advection of plasma density perturbations with imbedded electric charges by the sheared plasma flow inevitably alters such instabilities (e.g. see Fig. VII.16, VII.18). For the case of drift waves, the situation is very different. In this case, the electric field and related $\vec{E}\times\vec{B}$ drifts are due to the largely "reversible" response of the fast parallel electron dynamics on plasma density perturbations. Even though the advection of plasma density perturbations by the sheared flow changes the "landscape" of density perturbations, the distribution of the electric charges has virtually no "memory" and, therefore, the sheared flow makes a very mild impact on the growth rate of the drift wave instabilities. We notice that the manifestation of the different impact of the velocity shear on the drift wave- and the magnetic

drift-driven plasma instabilities can be also seen in the dependence of the corresponding eigenfunctions. For example, comparing the impact of the velocity shear on the eddies related to the eigenfunctions of the RT (Fig. VII.17) and the drift wave (Fig. VII.22) instabilities, one can see that unlike the RT instability, the eddies corresponding to the drift wave instability are not stretched by the sheared flow at all. However, the number of eddies is reduced and their center is shifted along x-coordinate.

Nonetheless, even though the impact of the velocity shear on the growth rate of the resistive drift wave instability is mild, a significant reduction of the radial extent of the drift wave eddy, caused by the velocity shear, can also result in a reduction of anomalous cross-field transport.

Next, we discuss the absence of solutions of Eq. (VII.93) at a rather large velocity shear, $|V_0'| > |V_0'|_{loc}$. We can interpret this effect within the eikonal approximation, where the wave packet can be considered as an effective "particle", dynamic of which is described with the "Hamiltonian" $\omega(k_x, x) = \omega_*(x)(1 + k_x^2\rho_s^2 + k_y^2\rho_s^2)^{-1} + V_0' k_y x$ and the canonical variables x and k_x. To have a localized solution of the wave packet, the motion of the "particle" should be bounded by two turning points corresponding to $k_x = 0$. To make it happen, the function $\omega(k_x = 0, x)$ must have at least one extremum. For the case where $\omega_*(x) = \hat{\omega}_* \cosh^{-2}(x/w)$, it is easy to show that this is only possible for

$$|V_0'| < |V_0'|_{loc} \approx \frac{4}{3^{3/2}} \frac{\hat{\omega}_* / (w k_y)}{1 + \rho_s^2 k_y^2}. \qquad \text{(VII.94)}$$

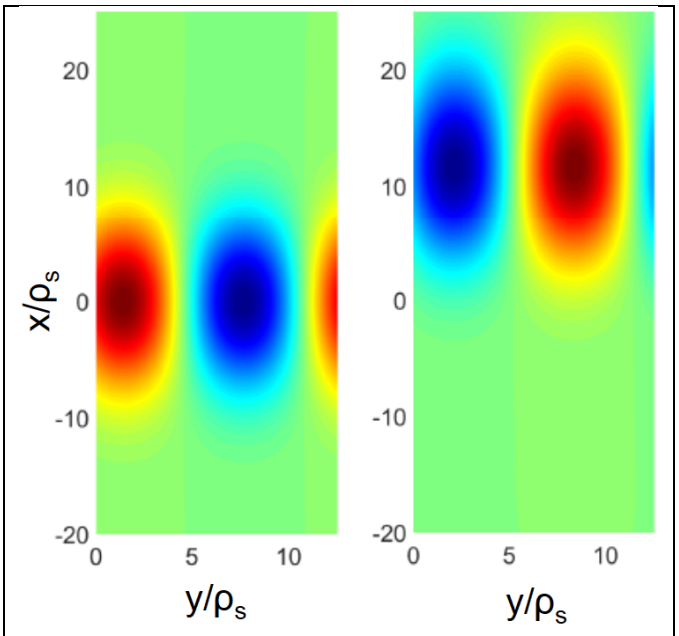

Fig. VII.22. Eddies corresponding to the eigenfunctions found from numerical solutions of Eq. (VII.93) for $V_0' = 0$ (left) and $|V_0'|/|V_0'|_{loc} = 0.8$ (right). Other parameters used in these simulations are: $k_y\rho_s = 0.5$, $w/\rho_s = 30$, and $\nu_{||}/\hat{\omega}_* = 50$. Reproduced with permission from [66], © AIP Publishing 2020.

Beyond this limit, no localized solution of Eq. (VII.93) exists. Estimate (VII.94) is in a reasonable agreement with the results of numerical simulations (e.g. see Fig. VII.22). We notice that in [83], the evolution of a drift wave packet was considered for the case of $\omega_*(x) = \text{const}$. but a more complex structure of the velocity shear.

Unfortunately, in the tokamak experiments, it is virtually impossible to distinguish the impact of the plasma flow on different modes. Therefore, experimental confirmation of the impact of the velocity shear on the plasma instabilities is usually deduced from the reduction of anomalous plasma transport. In some experiments, the external biasing of the plasma interior imposes the velocity shear [84], [85]. Arguably, such experiments provide the most "clean" experimental data on the impact of the velocity shear on the suppression of plasma turbulence. From Fig. VII.23 one can see, in particular, that strong shear of the radial electric field for the

"H-mode" case strongly suppresses the radial plasma particle flux.

Overall, it is widely accepted that shear of plasma flow results in a strong reduction of turbulent plasma transport and, in particular, is a key ingredient of establishing the high confinement regime (H-mode) (e.g. see [86], [87] [88], [60], [89], [90], [91] and the references therein).

So far we consider an impact of the so-called Zonal Flow (ZF) on plasma instabilities. ZF is a quasi-stationary plasma flow (sketched in Fig. VII.8), which can be driven, for example, by plasma biasing. However, in tokamaks, the sheared poloidal plasma flow can also be related to intrinsic low frequency (~10 kHz) toroidally symmetric plasma oscillations (recall Fig. VII.6): the Geodesic Acoustic Mode (GAM), see [35], [36] and the references therein. The physics of the GAM is rather simple: the compressibility of the toroidally symmetric $\vec{E}\times\vec{B}$ plasma flow causes a poloidaly asymmetric plasma pressure perturbation, $\tilde{P}$, and the corresponding diamagnetic current across magnetic flux surfaces, $\tilde{\vec{J}} \propto \vec{B}\times\tilde{P}$. This current is not divergence-free due to toroidal effects. It reverses the sign of the electric field and, finally, results in plasma oscillations, GAM. For a relatively large safety factor q, which is typical for the edge plasma, the plasma dynamics along the magnetic field lines can be ignored and, in the simplest case, the expression for the GAM frequency reads:

$$\omega_{GAM}^2 = 2\gamma P_0 / \rho_0 R^2, \qquad \text{(VII.95)}$$

where P_0 and ρ_0 are the unperturbed plasma pressure and density, R is the tokamak major radius and γ is the ratio of the specific heats.

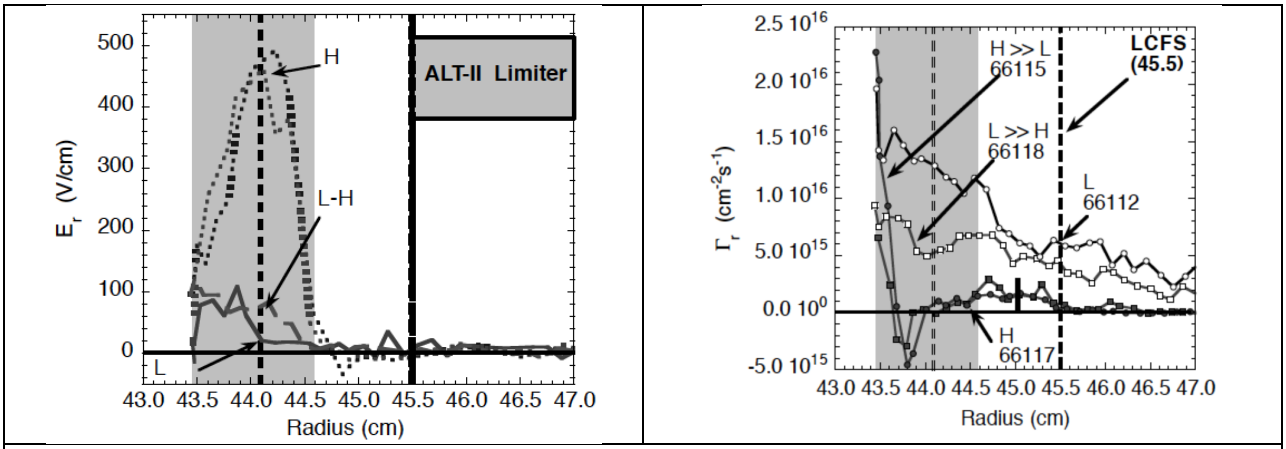

Fig. VII.23. Experimental data from the TEXTOR tokamak obtained with the external plasma biasing. On the left: The profiles of the radial electric field for different cases: "L-mode", "H-mode", and "L to H transition"; On the right: the radial plasma fluxes for "L-mode", "H-mode", just before the L to H ("L>>H") and H to L ("H>>L") transitions. Reproduced with permission from [84], © IAEA 2010.

VII.3 Nonlinear effects and anomalous transport

In the previous section, we considered some plasma instabilities which can be important for plasma transport at the edge and in the SOL of a tokamak. We also considered possible stabilizing effects, which are the magnetic and velocity shear. However, in some cases, strong magnetic shear (e.g. in the vicinity of the X-point) can facilitate instabilities. In this section, we

discuss some features of anomalous plasma transport associated with these instabilities as well as the available stabilizing effects.

To be more precise, we will not discuss any particular scaling of anomalous cross-field transport coefficients in the edge plasmas (e.g. see [92]). Instead, we consider the main features governing anomalous transport in the edge plasma. The reason for this can be explained as follows. First, the most common approach to estimating analytically the impact of a particular unstable mode on anomalous transport is based on a local (at a given flux surface) diffusive approximation where the transport coefficients (say, the particle diffusion coefficient, D) are described by the expression

$$D \approx \gamma k_{\perp}^{-2}, \qquad \text{(VII.96)}$$

where γ and $k_{\perp}$ are the characteristic growth rate and cross-field wave number of the mode (e.g. see [92], [93] and the references therein). However, as we found in the previous section, in edge plasma different modes can be unstable simultaneously and it is virtually impossible to find their contribution to the anomalous cross-field transport coefficients, which depend not only on plasma parameters and their radial derivatives but also on the shear of plasma flow velocity. We will see that sheared plasma flow can be generated by plasma turbulence itself (e.g. see [94], [60], [90], [91] and the references therein). Moreover, the interplay of the sheared plasma flow generation by turbulence and the impact of such a flow on the turbulence itself can result in time-depended fluctuations of the amplitudes of plasma turbulence and shear of plasma flow velocity [95]. In addition, experiments show that a large contribution of edge plasma transport is from radial advection (predominantly, at the outboard side of the torus) of coherent filamentary structures with plasma density and temperature higher than those in the ambient plasma, the so-called "blobs" (see Fig.VII.24, [98], [100] and the references therein). It is widely accepted that blobs are propelled by $\vec{E} \times \vec{B}$ drift due to plasma polarization caused by magnetic drifts (the so-called ballooning effect) [101], [102].

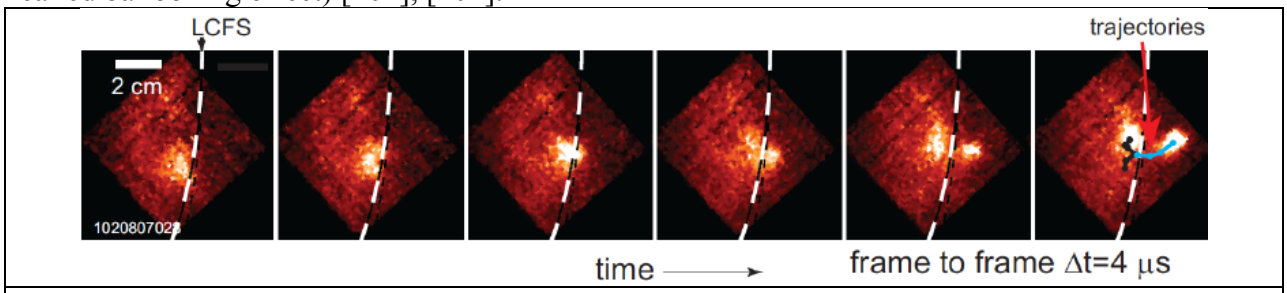

Fig. VII.24. Motion of a blob, seen as the bright spot, in the C-Mod tokamak [96] observed with the Gas-Puff Imaging (GPI) diagnostic [97]. The GPI is based on a higher radiation intensity of neutral hydrogen in the regions with enhanced plasma density and temperature. J. P. Terry, private communication, 2018.

We notice that such "blobby" anomalous cross-field plasma advection cannot be described *a priory* by a local theory describing the plasma parameters at a particular flux surface. As a result of such plasma advection on the outboard side of the torus, plasma turbulent transport and plasma parameters at the edge become strongly dependent on the magnetic configuration and for the case of double null configuration (which effectively disconnects the inboard and outboard sides of the torus due to the X-point effects), plasma transport and the magnitude of the turbulent fluctuations on the inboard side becomes much weaker than on the outboard one (see Fig. VII.25).

Finally, it was found experimentally that the SOL midplane width, and, therefore, midplane plasma transport, can also strongly depend on divertor conditions and for the detached divertor case, the width is about two times larger than for the attached one (see Fig. VII.26). We note that so far there is no clear theoretical explanation of such an effect, although there is an indication that neutrals, density of which strongly increases in the detached divertor regime, can play some role in the modification [105] and even enhancement of plasma transport, in particular, due to reduction of the shear of the plasma flow [106].

Thus, taking into account so many different factors which can alter anomalous edge plasma transport, we can conclude that the only plausible way to estimate anomalous transport with some confidence is to use 3D edge plasma turbulent codes such as BOUT++ [107], XGC1 [108], GENE [109], Gkeyll [110], JOREK [111] and some others. These codes are based on different plasma models (e.g. BOUT++ and JOREK codes are based, respectively, on the fluid and MHD plasma equations, whereas XGC1, GENE and Gkeyll are gyrokinetic codes which, however, also have some differences).

As a result, their application limits are different (for example, JOREK is usually used to simulate ELM, whereas the others are usually used for the simulation of edge plasma turbulence). We will discuss some results coming from these codes later. However, we notice that the codes used for the simulation of edge plasma turbulence, in most cases cannot describe edge plasma transport on the relevant time scale, due to both the lack of some important physics needed for such a description and the limitation of current computational resources. Therefore, they often use the plasma parameter profiles taken either from experimental data or from the results of simulation of the edge plasma parameters with 2D edge plasma transport codes such as SOLPS or UEDGE.

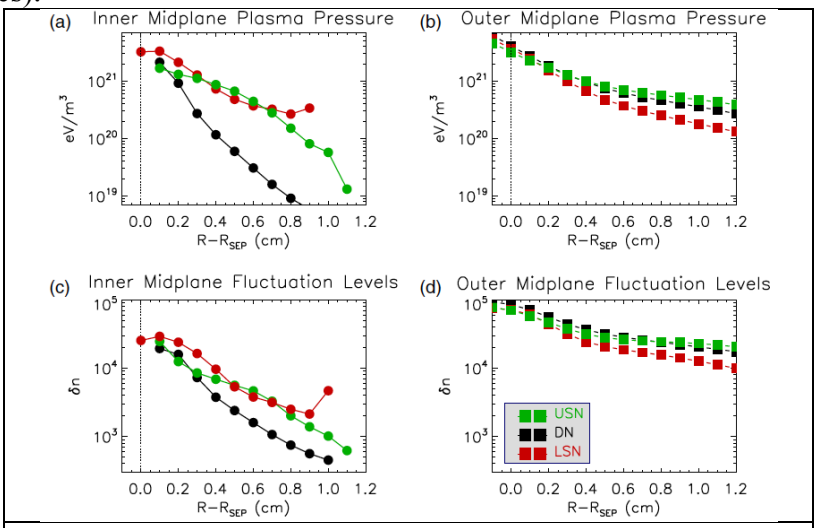

Fig. VII.25. Distribution of plasma pressure and fluctuation level at the inner and outer midplanes of the SOL for upper- and low-single null (USN, LSN) and double-null (DN) magnetic configurations. Reproduced with permission from [103], © IAEA 2004.

Now we consider the main features, outlined above, which govern anomalous transport in the edge plasma.

VII.3.1 Generation of sheared plasma flow via plasma turbulence

As we found in the previous section, in strongly magnetized plasma, the unstable modes are characterized by a strong anisotropy, which is characterized by the inequality $|k_{||}|<<|\vec{k}_{\perp}|$. Therefore, within some limitations, the interaction of the plasma waves and plasma turbulence can, in general, be considered two-dimensional (2D). This feature makes the dynamics of magnetized plasma somewhat similar to that of geophysical fluids [112]. However, it is known since a long time ago that the main features of the turbulence in 2D fluids (including the

magnetized plasma) are very different from the predictions following from such a cornerstone of three-dimensional (3D) fluid turbulence as the Kolmogorov turbulence model. The main reason for this is that in addition to the energy, in 2D fluids there is an extra invariant, enstrophy (e.g. see [113], [114], [115]), which prevents the energy cascade to and the energy dissipation at small scales, which happens in the Kolmogorov 3D turbulence model.

As an illustration, we consider the so-called Charney-Hasegawa-Mima (CHM) model [116], [115], which is the simplest nonlinear model describing both the atmospheric Rossby and the magnetized plasma drift wave dynamics. We consider plasma embedded into a straight constant magnetic field (in the z-direction) and having constant electron temperature and cold ions. We will assume that the perturbation of the electron density, $\tilde{n}_e$, obey the Boltzmann relation which we will approximate as follows

$$\tilde{n}_e = n(x)\{\exp(\tilde{\phi}) - 1\} \approx n(x)\tilde{\phi}, \qquad \text{(VII.97)}$$

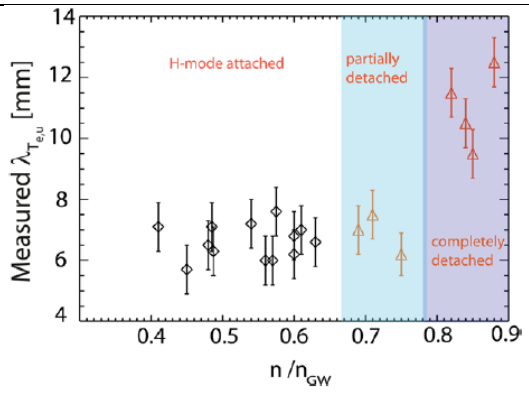

Fig. VII. 26. Outer SOL electron temperature decay length for the attached and detached outer divertor conditions. Reproduced with permission from [104], © IOP Publishing 2015.

where $n(x)$ is the unperturbed plasma density depending on the "radial" coordinate x. The ion velocity can be found from Eq. (VII.8), (VII.9). Keeping nonlinear terms, we find

$$\vec{V}_i = \vec{V}_{\vec{E}\times\vec{B}} - \left(\frac{\partial}{\partial t} + \vec{V}_{\vec{E}\times\vec{B}}\cdot\nabla\right)\frac{cT_e\nabla_\perp\tilde{\phi}}{B\Omega_{Bi}}, \qquad \text{(VII.98)}$$

where $\vec{V}_{\vec{E}\times\vec{B}} = (cT_e/eB)\vec{e}_z\times\nabla\tilde{\phi}$. Substituting the expression (VII.98) into ion the continuity equation and assuming quasi-neutrality, we arrive at the CHM equation

$$\left(\frac{\partial}{\partial t} + \vec{V}_{\vec{E}\times\vec{B}}\cdot\nabla\right)\left(\tilde{\phi} - \rho_s^2\nabla_\perp^2\tilde{\phi}\right) - \frac{cT_e}{eB}\frac{d\ell n\{n(x)\}}{dx}\vec{e}_y\cdot\nabla\tilde{\phi} = 0, \qquad \text{(VII.99)}$$

which in the linear case gives the drift wave frequency (VII.16).

Similar to the 2D Euler equation [114], the CHM equation has two exactly conserved integrals: energy, E, and enstrophy, En, which can be expressed in the continuum and spectral forms as follows:

$$E = \int\left\{(\rho_s\nabla_\perp\tilde{\phi})^2 + \tilde{\phi}^2\right\}d\vec{r}_\perp \equiv \int\left\{(1+\rho_s^2k_\perp^2)|\tilde{\phi}_{\vec{k}_\perp}|^2\right\}d\vec{k}_\perp, \qquad \text{(VII.100)}$$

$$En = \int\left\{(\rho_s^2\nabla_\perp^2\tilde{\phi})^2 + (\rho_s\nabla_\perp\tilde{\phi})^2\right\}d\vec{r}_\perp \equiv \int\left\{(1+\rho_s^2k_\perp^2)\rho_s^2k_\perp^2|\tilde{\phi}_{\vec{k}_\perp}|^2\right\}d\vec{k}_\perp. \qquad \text{(VII.101)}$$

From Eq. (VII.100), (VII.101) it follows that unlike the Kolmogorov model of 3D fluid turbulence, to conserve both integrals in the CHM model, the energy must be cascaded to large spatial scales (small $|\vec{k}_\perp|$) whereas the enstrophy to the small ones (large $|\vec{k}_\perp|$). Thus, we see that the generation of large-scale structures from small-scale fluctuations is inherent for 2D turbulence. However, these conservation laws tell us nothing about the generation of the zonal flows, which can suppress the plasma instabilities. Generally speaking, these large-scale structures can be large-scale convective cells facilitating anomalous cross-field plasma transport [117]. For this reason, the topic of zonal flow generation from drift wave turbulence have

received so much attention from both theory (e.g. see [94], [118], [60], [119] and the references therein) and experiment (e.g. see reviews [90], [91]).

Just to give an idea of theoretical approaches used in these studies, we will follow [94] and consider the CHM equation modified by the presence of a weak zonal flow. For this purpose, we separate the perturbation of the electrostatic potential into two parts: $\tilde{\phi}(\vec{r},t)=\tilde{\phi}_{dw}(\vec{r}_\perp,z,t)+\tilde{\phi}_{zf}(x,t)$, where $\tilde{\phi}_{dw}(\vec{r}_\perp,z,t)$ and $\tilde{\phi}_{zf}(x,t)$ describe respectively the drift waves and zonal flow. Such a separation is needed because the z-dependence of $\tilde{\phi}_{dw}$ justifies the Boltzmann relation for the perturbed plasma density and $\tilde{\phi}_{dw}$, even though the CHM equation *per se* contains no direct z-dependence. This is to the contrary to $\tilde{\phi}_{zf}(x,t)$, which has no z-dependence and, therefore, does not enter into the Boltzmann relation, although it contributes to the $\vec{E}\times\vec{B}$ plasma flow. Keeping this in mind and using only $\tilde{\phi}_{dw}$ in Eq. (VII.97) but total $\tilde{\phi}$ in Eq. (VII.98), we arrive at the following modified Hasegawa-Mima equation [94], [118]:

$$\frac{\partial}{\partial t}\left(\tilde{\phi}_{dw}-\rho_s^2\nabla_\perp^2\tilde{\phi}\right)+\left(\vec{V}_{zf}+\vec{V}_{dw}\right)\cdot\nabla\left(\tilde{\phi}_{dw}-\rho_s^2\nabla_\perp^2\tilde{\phi}\right)-\frac{cT_e}{eB}\frac{d\ell n\{n(x)\}}{dx}\vec{e}_y\cdot\nabla\tilde{\phi}=0\,, \quad \text{(VII.102)}$$

where $\vec{V}_{zf}=(cT_e/eB)\vec{e}_z\times\nabla\tilde{\phi}_{zf}$ and $\vec{V}_{dw}=(cT_e/eB)\vec{e}_z\times\nabla\tilde{\phi}_{dw}$.

For the case where one drift wave with the amplitude $\tilde{\phi}_{dw}^{(1)}$, wavenumber $\vec{k}^{(1)}$ and frequency given by expression (VII.16) dominates, Eq. (VII.102) describes modulation, or in a more general case, parametric instability of this wave, which describes the excitation of $\tilde{\phi}_{zf}$. The growth rate of such instability, γ_{zf}, for the case where $k_{zf}\rho_s<<1$ (here k_{zf} is the x-component of the wavenumber of the zonal flow) we have [94], [118]:

$$\gamma_{zf}=\frac{cT_e}{eB}\frac{|\tilde{\phi}_{dw}^{(1)}|\,k_{zf}k_y^{(1)}}{\sqrt{1+k_1^2\rho_s^2}}\sqrt{1+\rho_s^2\left((k_y^{(1)})^2-3(k_x^{(1)})^2\right)}\,, \quad \text{(VII.103)}$$

which, in particular, shows that for the case of $k_1^2\rho_s^2<<1$, the drift wave is always unstable and generates a zonal flow. Analysis of the dynamics of uncorrelated drift wave packets performed in [94] also demonstrates the possibility of the generation of zonal flows. In [120] it was shown that in addition to the exact integrals of the CHM equation (the energy and the enstrophy) there is also a third "approximate" integral, I, which, however, becomes exact for the case of the resonant triad interactions (see also [121] and the references therein). This integral can only be expressed in a spectral form:

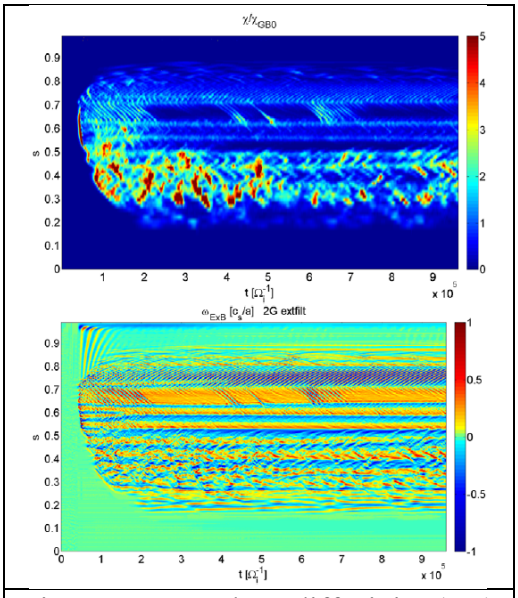

Fig. VII.27. Ion heat diffusivity (top) and the shearing rate of zonal flow (bottom) found from numerical simulation of ITG turbulence in ITER as the function of time and normalized poloidal magnetic flux. Reproduced with permission from [122], © IOP Publishing 2013.

$$I = \int \frac{\eta(\vec{k}_\perp)}{k_y}\left(1+\rho_s^2 k_\perp^2\right)^2 |\tilde{\phi}_{\vec{k}_\perp}|^2 \, d\vec{k}_\perp , \qquad \text{(VII.104)}$$

where $\tilde{\phi}_{\vec{k}_\perp}$ is the Fourier component of drift wave fluctuations and

$$\eta(\vec{k}_\perp) = \arctan\left(\frac{k_x + \sqrt{3}k_y}{\rho_s k^2}\right) - \arctan\left(\frac{k_x - \sqrt{3}k_y}{\rho_s k^2}\right). \qquad \text{(VII.105)}$$

It was shown that even approximate conservation of I ensures that the energy of the turbulence described by the CHM equation is transferred to a very anisotropic zonal flow with $k_x >> k_y$ [120].

We notice that GAM, which in the edge plasma can be as efficient for the damping of plasma turbulence as the zonal flows, can also be excited by nonlinear processes associated with plasma turbulence [36]. The turbulence-induced generation of a zonal flow it now routinely observed in large-scale 3D plasma turbulence simulations (e.g. see [60] and the references therein).

As an example, in Fig. VII.27 one can see the ion heat diffusivity and the shearing rate of the zonal flow found from the numerical simulation of ITG turbulence in ITER. One can clearly see both the variation of the sign of the shearing rate along with the normalized poloidal magnetic flux and the reduction of the ion heat diffusivity for the case of a fully developed zonal flow at a later time.

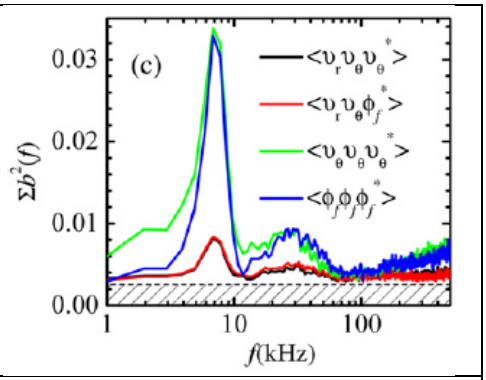

Fig. VII.28. The summed cross- and auto-bicoherences of electric field fluctuations measured by probe array at the edge of HL-2A tokamak. Reproduced with permission from [123], © IOP Publishing 2008.

There is also a significant body of experimental data supporting the generation of both zonal flows and GAM due to nonlinear processes associated with plasma turbulence (e.g. see [90], [91] and the references therein). As an example, in Fig. VII.28 one can see summed cross- and auto-bicoherences, $\hat{b}^2(f, f_{GAM} - f)$, of the electric field fluctuations measured by a probe array at the edge of the HL-2A tokamak. Very distinct peaks at the frequency $f_{GAM} \approx 7\,\text{kHz}$, exhibited by all three curves, demonstrate a strong coupling of GAM to the broadband plasma turbulence.

Finally, Fig. (VII.14) shows that the zonal flow goes over the entire poloidal circuit. However, recent experimental data [124] suggest that this might be not always the case and the co- and counter-wise streams can gradually close on each other forming, as a result, a poloidally extended convective cell at the outer side of the torus, which, nonetheless, can still be rather efficient in turbulence suppression at the outer side of the torus.

VII.3.2 "Blobs"

Meso-scale plasma structures which are now called blobs were occasionally observed experimentally for a long time as, in particular, large spikes of the ion saturation current collected by electrostatic probes at the edge of tokamaks (e.g. see [125] and Fig. VII.29).

However, only after a very large plasma particle flux to the main chamber wall was discovered in the C-Mod tokamak [127] and it became clear that such a flux is incompatible with the diffusive nature of plasma transport [127], [101], the physics of blobs became one of the central topics of the edge plasma studies.

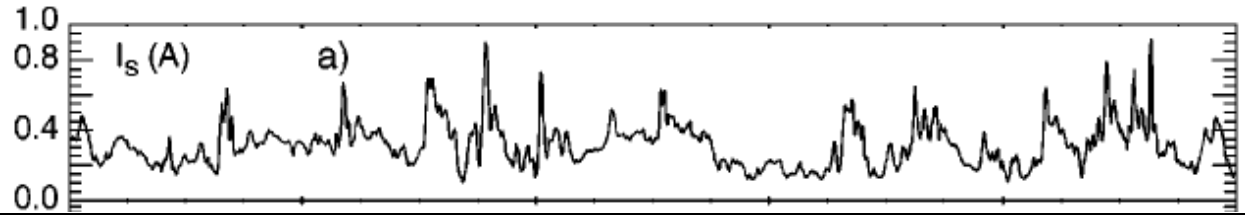

Fig. VII.29. Time dependence of the ion saturation current on the probe situated in the SOL of the DIII-D tokamak. Reproduced with permission from [126], © AIP Publishing 2001.

As of today, the blobs are observed in virtually all magnetic fusion devices including both tokamaks and stellarators [128], [129] [130], [131] and there is vast amount of literature dedicated to different experimental and theoretical aspects of blobby transport (e.g. see review papers [128], [98], [100]). As a matter of fact, the physical reason for the radial advection of blobs (which are the filamentary structures extended along the magnetic field, see Fig. VII.29) is simple [102].

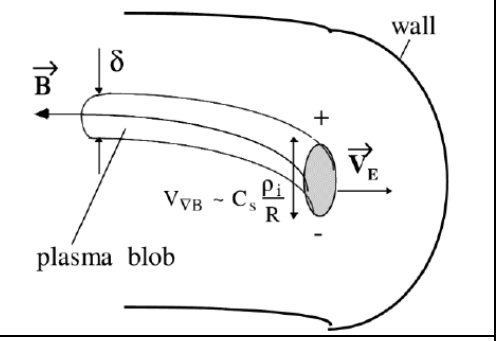

Fig. VII.30. Schematic view of the filament's polarization and advection due to magnetic and $\vec{E}\times\vec{B}$ drifts. Reproduced with permission from [102], © Elsevier 2001.

Consider an isolated plasma filament situated in a vacuum (or in very low density plasma) sketched in Fig. VII.30. Then magnetic drifts of the electrons and ions will result in the polarization of the filament and the formation of a vertical (along the major tokamak axis) electric field (for simplicity, we ignore the effect of the magnetic shear). Such an electric field will cause outward advection of the filament (see Fig. VII.24) due to $\vec{E}\times\vec{B}$ drift.

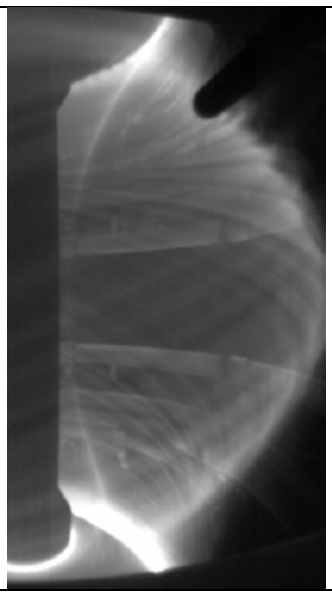

Fig. VII.31. Visible light image of blob filaments from MAST tokamak. Reproduced with permission from [135], © IAEA 2007.

Therefore, in tokamaks, blobs are mainly observed at the outer side of the tours. The strength of the vertical electric field is altered by the parallel electric current. Different theoretical models for such a current, giving different scalings for the blob speed, were used over the years including the sheath- and X-point-limited current, and the "inhibited" current (see the review papers [98], [100] for details).

In the latter case, the blobs can reach the highest speed, which, according to the numerical simulations [132], for $n_b >> n_a$ can be estimated as

$U_{max} \approx \sqrt{2(T_e + T_i)/M}\sqrt{(n_b/n_a)(\delta_b/R)}$, where n_b and n_a are plasma density in the blob and in the ambient plasma, δ_b is the initial cross-field size of the blob.

For typical tokamak edge plasma parameters we find $U_{max} \sim 1\,km/s$, which is, in a ballpark, consistent with the experimental observations (e.g. see [126], [133]). For sheath-limited parallel electric current, the scaling for the blob velocity reads $U_b \propto \delta_b^{-2}$ [102]. The available experimental data seem to support both these scaling [134]. The filamentary structure of the blob was confirmed by direct observations with fast cameras (e.g. see Ref. [135], [137], [138]). As an example, in Fig. VII.31 one can see a snapshot made in an L-mode discharge in the MAST tokamak, which reveals multiple filamentary structures.

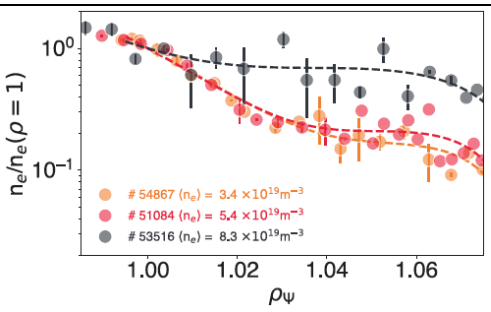

Fig. VII.32. Formation of the "shoulder" on averaged plasma density in the SOL at high plasma density. Reproduced with permission from [140], © IAEA 2017.

We notice that blobs are seen in both the L- and H-modes (e.g. see [137]) (in between ELMs) and in both cases, the blobs dominate far SOL plasma transport [126]. However, recent experimental data show that blobs exist not only at the outer boundary of tokamaks but also in the divertor volume [58] although the impact of these blobs on plasma transport is not yet clear.

Numerical simulations show that the shape of the blobs, in the course of their radial advection, can be significantly deformed due to effects associated with the Rayleigh-Taylor and Kelvin-Helmholtz instabilities [98]. Also, 2D and 3D simulations demonstrate that blobs can be effectively disintegrated by sheared background plasma flow [138] and the onset of the resistive drift wave instability [139].

Usually, blobby transport is enhanced when the plasma density approaches the density limit. One of the typical manifestations of such enhancement is the formation of the so-called "shoulder" on averaged plasma density profile in the far SOL region (see Fig. VII.32).

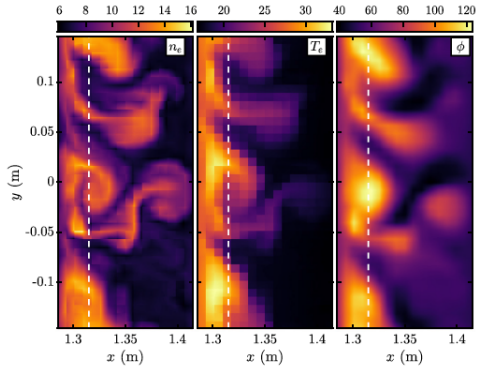

Fig.VII.33. Snapshots of plasma parameters at the outer midplane found from numerical simulations. Reproduced with permission from [141], © AIP Publishing 2019.

Modeling of edge plasma transport with turbulence codes also shows both blob formation and advection. As an example, in Fig. VII.33 one can see the snapshots of the distribution of edge plasma parameters, having clear features of blobs, found with the gyrokinetic code XGC1 [141] (white dashed line is the effective separatrix).

Although the dynamics of individual blobs in the SOL is understood rather well, the formation mechanism of large density blobs, in particular, those which are observed inside the separatrix, recall Fig. (VII.24), is not clear. In [142] it was shown that the 1D version of the modified Hasegawa-Mima equation allows the solution in the form of a train of plasma density "blobs" propagating in poloidal direction, which resembles the experimental data, see Fig.

(VII.34), on the dynamics of nonlinear drift waves [15]. However, as of today, there is no direct experimental confirmation that plasma density blobs can be formed in the course of nonlinear evolution of drift waves.

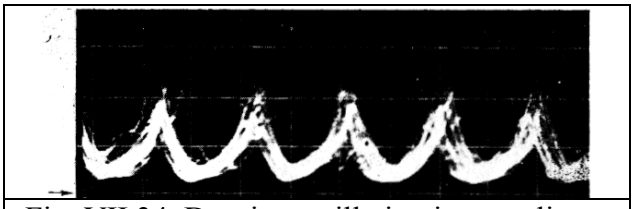

Fig. VII.34. Density oscillation in a nonlinear drift wave. The arrow on the left corresponds to zero plasma density. Reproduced with permission from [15], © Springer 1967.

We notice that strong blobby transport poses a serious problem for the application of 2D edge plasma transport codes like SOLPS or UEDGE for interpretation of the experimental data [99]. The issue is that these codes deal with average plasma parameters and their results are compared with average experimental data on plasma density, temperature, etc. However, for strongly nonlinear functions such as the dependence of the rate constants of atomic processes on electron temperature, $K(T_e)$, we have $\langle K(T_e)\rangle \neq K(\langle T_e\rangle)$, where $\langle ...\rangle$ means time averaging. As a result, strong intermittent fluctuations of the plasma parameters, associated with blobs, will inevitably cause a departure of the averaged experimental data from the simulation results.

VII.3.3 3D edge plasma turbulence modeling

Today quite a few codes of different sophistication are available for edge plasma turbulence simulation: BOUT++ [149], XGC1 [108], TOKAM3X [143], GBS [144], GDB [32], GRILLIX [145], Gkeyll [110], and some others.

These codes are used for both modeling some particular experiments and for studying the general characteristics and dependences of edge plasma turbulence. For example, in Fig. (VII.35) one can see a very good agreement of experimental data on the parallel Mach number of the plasma flow in the SOL of the COMPASS tokamak with the results of the modeling of the impact of plasma turbulence and macroscopic $\vec{E}\times\vec{B}$ drifts on parallel plasma flows, performed with the TOKAM3X fluid turbulence code [143]. Another example of a comparison of modeling results and experimental data is shown in Fig. (VII.36). Here one can see the probability density function for the density fluctuations from the Helimak toroidal device and the results of the numerical simulations performed with the Gkeyll gyrokinetic code.

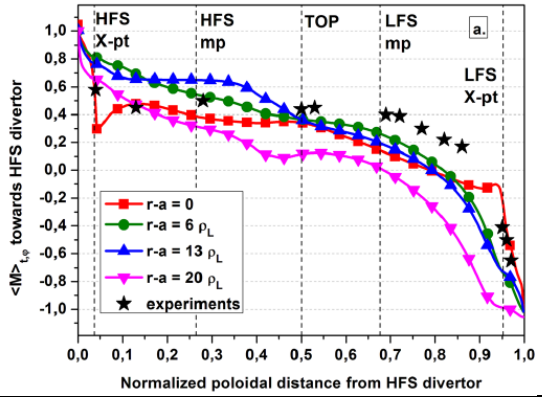

Fig. (VII.35) Comparison of experimental data and simulation results on the parallel Mach number of the plasma flow in the SOL of the COMPASS tokamak. Here HFS and LFS stand for the high- and low- field sides of the torus. Reproduced with permission from [143], © IAEA 2017, experimental data from Asakura N. et al, *J. Nucl. Mater.* **365** 41–51.

Even though all the curves in Fig. (VII.36) exhibit non-Gaussian features (typical for blobby transport), the simulations do not reproduce the long tail of the density fluctuations observed in the experiment. Another important area of the application of 3D plasma turbulence

codes is related to the simulation of the width, λ_q, of the part of the SOL, where the heat flux is transported to the divertor target. This parameter is of particular importance for ITER because it largely determines the heat load on the divertor target. Recently established experimental scaling predicts that in H-mode in between ELMs, $\lambda_q \propto I_p^{-1} \propto B_{pol}^{-1}$, where I_p is the tokamak plasma current and B_{pol} is the strength of the poloidal magnetic field [146].

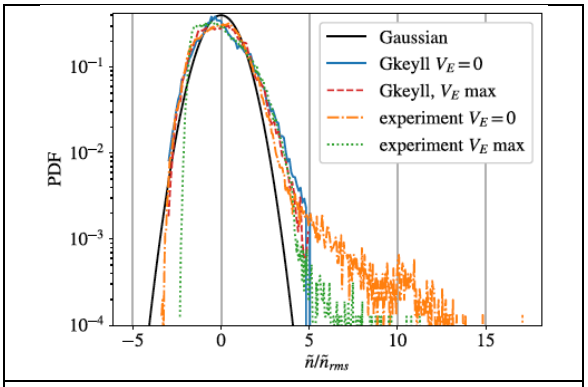

Fig. (VII.36). Probability density functions for density fluctuations. Reproduced with permission from [110], © AIP Publishing 2019.

In [147] this scaling was attributed to ion drifts in the tokamak magnetic field (with no turbulent impact on the ion dynamics) so that λ_q becomes of the order of the poloidal gyroradius of ions. Recently, this scaling was reproduced for current tokamaks by the fluid BOUT++ and gyrokinetic XGC1 plasma turbulence codes (see Fig. VII.37).

Interestingly, both codes predict a large departure of λ_q from the experimental scaling for ITER (see Fig. (VII.37). However, the physics of this is not clear yet and further studies are needed to confirm these results. In [149] it was speculated that the transition from drift- to turbulence-dominated processes that set λ_q occurs in next step tokamaks due to the larger size and stronger magnetic field strength.

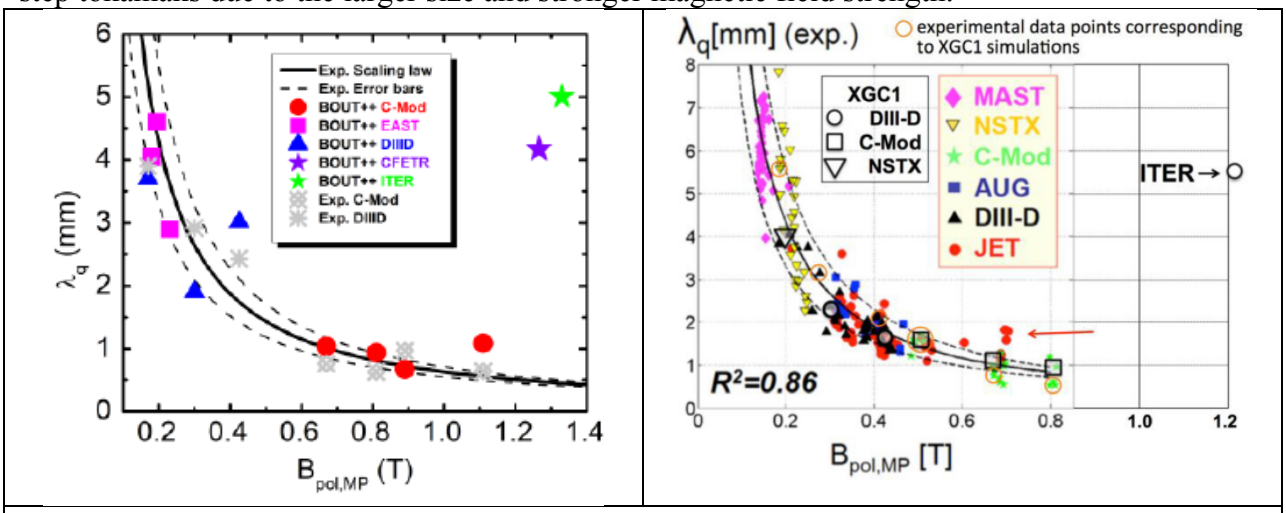

Fig. (VII.37). Predictions of λ_q for different existing tokamaks and ITER found (left) with the BOUT++ (Reproduced with permission from [148], © IAEA 2018) and (right) XGC1 (Reproduced with permission from [108], © IAEA 2013) plasma turbulence codes.

Conclusions for Chapter VII

In this chapter, we reviewed the basic theory of plasma waves responsible for anomalous plasma transport, considered their main destabilizing mechanisms and presented some experimental data confirming the theoretical and simulation results. The situation with theoretical analysis and

predictions of anomalous cross-field transport is more complex and as of today, we only have a basic theoretical understanding of the processes governing anomalous plasma transport, although there is a large amount of experimental data and simulation results supporting these ideas. Nonetheless, at present, practically all results of edge plasma transport simulation performed with 2D codes such as SOLPS or UEDGE, are based either on the usage of the anomalous transport coefficients fitting the edge plasma parameter profiles observed in experiments or on the scoping studies of an impact of the transport coefficients on edge plasma performance for the cases where there is no available data yet (e.g. ITER simulations, see Chapter IX).

References for Chapter VI I

[1] L. I. Rudakov, R. Z. Sagdeev, "Oscillations of an inhomogeneous plasma in a magnetic field", Sov. Phys. JETP **37** (1960) 952-954.

[2] B. B. Kadomtsev, "Plasma Turbulence", Academic Press (1965).

[3] W. M. Tang, "Microinstability theory in tokamaks", Nucl. Fusion **8** (1978) 1089-1160.

[4] W. Horton, "Turbulent transport in magnetized plasmas", Second Edition, World Scientific, 2018.

[5] L. D. Landau and L. M. Lifshitz "The Classical Theory of Fields", Course of Theoretical Physics, Volume 2, Third Edition, Elsevier Ltd. 2009.

[6] L. D. Landau and L. M. Lifshitz "Quantum Mechanics (Non-Relativistic Theory)", Course of Theoretical Physics, Volume 3, Third Edition, Elsevier Ltd. 2005.

[7] E. M. Lifshitz and L. P. Pitaevskii "Physical Kinetics", Course of Theoretical Physics, Volume 10, Third Edition, Elsevier Ltd. 2008.

[8] S. I. Braginskii, "Transport processes in plasma", in Reviews of Plasma Physics, edited by M. A. Leontovich (Consultants Bureau, New York, 1965), Vol. 1, p. 205.

[9] A. B. Mikhailovskii and V. S. Tsypin, "Transport equations and gradient instabilities in a high pressure collisional plasma", Plasma Phys. **13** (1971) 785-798.

[11] A. N. Simakov and P. J. Catto "Drift-ordered fluid equations for field-aligned modes in low-b collisional plasma with equilibrium pressure pedestals", Phys. Plasmas **10** (2003) 4744-4757.

[12] P. J. Catto and A. N. Simakov "A drift ordered short mean free path description for magnetized plasma allowing strong spatial anisotropy", Phys. Plasmas **11** (2004) 90-102.

[13] J. R. Angus and S. I. Krasheninnikov "drift wave dispersion relation for arbitrary collisional plasma", Phys. Plasmas **19** (2012) 052504.

[14] H. Lashinsky "Landau damping and finite-length effects in universal plasma instabilities", Phys. Rev. Lett. **13** (1964) 47-50.

[15] N. S. Bruchel'nikova, R. A. Salimov, and Yu. I. Eidel'man, "Plasma turbulence in the presence of a drift instability", Sov. Phys. JETP **25** (1967) 548-556.

[16] H. W. Hendel, T. K. Chu, and P. A. Politzer, "Collisional Drift Waves-Identification, Stabilization, and Enhanced Plasma Transport.", Phys. Fluids **11** (1968) 2426-2439.

[17] P. A. Politzer "Drift instability in Collisionless Alkali Metal Plasmas", Phys. Fluids **14** (1971) 2410-2425.

[18] H. L. Pécseli "Spectral properties of electrostatic drift wave turbulence in the laboratory and the ionosphere" Ann. Geophys. **33** (2015) 875-900.

[19] R. E. Rowberg and A. Y. Wong "Collisional Drift Waves in the Linear Regime", Phys. Fluids **13** (1970) 661-671.

[20] E. Mazzucato, "Low-frequency microinstabilities in the PLT tokamak", Phys. Fluids **21** (1978) 1063-1069.

[21] S. Banerjee, A. Diallo, and S. J. Zweben, "Observation of quasi-coherent edge fluctuations in Ohmic plasmas on National Spherical Torus Experiment", Phys. Plasmas **23** (2016) 044502

[22] J. C. Perez, W. Horton, K. Gentle, W. L. Rowan, and K. Lee, "Drift wave instability in the Helimak experiment", Phys. Plasmas **13** (2006) 032101.

[23] L. I. Rudakov, R. Z. Sagdeev, "On the instability of a nonuniform rarefied plasma in a strong magnetic field", Dokl. Akad. Nauk SSSR, **138**, (1961) 581–583.

[24] Z. X. Lu, E. Fable, W. A. Hornsby, C. Angioni, A. Bottino, Ph. Lauber, and F. Zonca,

"Symmetry breaking of ion temperature gradiant mode structure: From local to global analysis", Phys. Plasmas **24** (2017) 042502.
[25] H.-S. Xie and Y. Xiao, "Unconventional ballooning structures for toroidal drift waves", Phys. Plasmas **22** (2015) 090703.
[26] M. K. Han, Z.-X. Wang, J. Q. Dong and H. Du, "Multiple ion temperature gradient driven modes in transport barriers", Nucl. Fusion **57** (2017) 046019.
[27] S. Chandrasekhar "Hydrodynamics and Hydromagnetic Stability", Dover Publications, 1981.
[28] H. P. Furth, J. Killeen, and M. N. Rosenbluth, "Finite‐Resistivity Instabilities of a Sheet Pinch", Phys. Fluids **6** (1963) 459-484.
[29] B. Coppi, "Influence of gyration radius and collisions on hydrodynamic stability" Phys. Fluids **7** (1964) 1501-1516.
[30] B. A. Carreras, L. Garcia, P. H. Diamond, "Theory of resistive pressure‐gradient‐driven turbulence" Phys. Fluids **30** (1987) 1388-1400.
[31] P. N. Guzdar, J. F. Drake, D. McCarthy, A. B. Hassam, and C. S. Liu, "Three-dimensional fluid simulations of the nonlinear drift-resistive ballooning modes in tokamak edge plasmas", Phys. Fluids B **5** (1993) 3712-3727.
[32] B. Zhu, M. Francisquez, and B. N. Rogers, "Global 3D two-fluid simulations of the tokamak edge region: Turbulence, transport, profile evolution, and spontaneous E3B rotation" Phys. Plasmas **24** (2017) 055903.
[33] D. A. Baver, J. R. Myra, M. V. Umansky, "Linear eigenvalue code for edge plasma in full tokamak X-point geometry", Comp. Phys. Comm. **182** (2011) 1610-1620.
[34] J. Q. Xu, Y. Xu, X. D. Peng, J. Cheng, W. L. Zhong, M. Jiang, Z. C. Yang, O. Pan, Y. Liu, L. W. Yan, Z. H. Huang, Z. B. Shi, M. Xu, Q. W. Yang, X. T. Ding, X. R. Duan, Y. Liu and the HL-2A Team "Experimental observation of the transition between resistive ballooning modes and ion temperature gradient modes in the edge of the HL-2A tokamak", Nucl. Fusion **58** (2018) 036002.
[35] N. Winsor, J. L. Johnson, and J. M. Dowson, "Geodesic Acoustic Waves in Hydromagnetic Systems", Phys. Fluids **11** (1968) 2448-2450.
[36] K. Hallatschek, "Nonlinear three-dimensional flows in magnetized plasmas", Plasma Phys. Contr. Fusion **49** (2007) B137-B148.
[37] J. W. Connor, R. J. Hastie, and J. B. Taylor, "Shear, Periodicity, and Plasma Ballooning modes", Phys. Rev. Lett. **40** (1978) 396-399.
[38] X. Q. Xu, B .D. Dudson, P. B. Snyder, M. V. Umansky, H. R. Wilson and T. Casper, "Nonlinear ELM simulations based on a nonideal peeling–ballooning model using the BOUT++ code" Nucl. Fusion **51** (2011) 103040**.**
[39] W. B. Kunkel and J. U. Guillory, in Proceedings of the Seventh Conference on Phenomena in Ionized Gases, Belgrade, 1965, edited by B. Perovic and D. Tocsic (Gradjevinska Knjiga, Belgrade, Yugoslavia, 1966), Vol. II, p. 702.
[40] B. B. Kadomtsev, in Proceedings of the Seventh Conference on Phenomena in Ionized Gases, Belgrade, 1965, edited by B. Perovic and D. Tocsic (Gradjevinska Knjiga, Belgrade, Yugoslavia, 1966), Vol. II, p. 610.
[41] A. V. Nedospasov, A. G. Petrov, G. N. Fidel'man, "Plasma convection in the poloidal limiter shadow of a tokamak", Nucl. Fusion **25** (1985) 21-27.
[42] H. L. Berk, D. D. Ryutov, and Yu. A. Tsidulko, "Temperature-gradient instability induced by conducting end walls". Phys. Fluids B **3** (1991) 1346-1354.

[43] B. B. Kadomtsev, "Hydromagnetic Stability of a Plasma", in Reviews of Plasma Physics, Volume 2, p. 153. Edited by M. A. Leontovich. Published by Consultants Bureau, New York (1966).
[44] S. I. Krasheninnikov and A. I. Smolyakov "Current convective instability in detached divertor plasma", Phys. Plasmas **23** (2016) 092505.
[45] B. Coppi, G. Laval, R. Pellat, M. N. Rozenbluth "Convective modes driven by density gradients", Nucl. Fusion **6** (1966) 261-267.
[46] P. E. Stott, P. F. Little, and J. Burt, "Drift waves and plasma diffusion in a shear-stabilized q machine", Phys. Rev. Lett. **25** (1970) 996-999.
[47] T. M. Antonsen, Jr., "Stability of Bound Eigenmode Solutions for the Collisionless Universal Instability", Phys. Rev. Lett. **41** (1978) 33-36.
[48] M. Landreman, T. M. Antonsen, Jr., and W. Dorland "Universal Instability for Wavelengths below the Ion Larmor Scale", Phys. Rev. Lett. **114** (2015) 095003.
[49] B. B. Kadomtsev and O. P. Pogutse, in Reviews of Plasma Physics, edited by M. A. Leontovich (Consultants Bureau, New York, 1970), Vol. 5, p. 249.
[50] B. A. Carreras, P. W. Gaffney, H. R. Hicks, and J. D. Callen, "Rippling modes in the edge of a tokamak plasma" Phys. Fluids **25** (1982) 1231-1240.
[51] D. Farina, R. Pozzoli and D. Ryutov, "Effect of the magnetic field geometry on the flute-like perturbations near the divertor X point" Nucl. Fusion **33** (1993) 1315-1317.
[52] J. R. Myra, D. A. D'Ippolito, X. Q. Xu, and R. H. Cohen, "Resistive modes in the edge and scrape-off layer of diverted tokamaks", Phys. Plasmas **7** (2000) 4622-4631.
[53] D. D. Ryutov and R. H. Cohen, "Instability Driven by Sheath Boundary Conditions and Limited to Divertor Legs", Contr. Plasma Phys. **44** (2004) 168-175.
[54] J. R. Myra, D. A. D'Ippolito, and X. Q. Xu, "Drift wave instability near a magnetic separatrix", Phys. Plasmas **9** (2002) 1637-1645.
[55] R. H. Cohen, B. LaBombard, D. D. Ryutov, J. L. Terry, M. V. Umansky, X. Q. Xu and S. Zweben, "Theory and fluid simulations of boundary-plasma fluctuations", Nucl. Fusion **47** (2007) 612-625.
[56] F. Scotti, S. Zweben, V. Soukhanovskii, D. Baver and J. Myra "Divertor leg filaments in NSTX-U", Nucl. Fusion **58** (2018) 126028.
[57] O. Grulke, J. L. Terry, I. Cziegler, B. LaBombard2 and O. E. Garcia, "Experimental investigation of the parallel structure of fluctuations in the scrape-off layer of Alcator CMod", Nucl. Fusion **54** (2014) 043012.
[58] J. R. Harrison, G. M. Fishpool, A. J. Thornton, N. R. Walkden, and MAST team, "The appearance and propagation of filaments in the private flux region in Maga Amp Spherical Tokamak" Phys. Plasmas **22** (2015) 092508.
[59] J. L. Terry, S. Ballinger, D. Brunner, B. LaBombard, A. E. White, S. J. Zweben, "Fast Imaging of filaments in the X-point region of Alcator C-Mod" Nucl. Mater. Energy **12** (2017) 989-993.
[60] P. H. Diamond, S.-I. Itoh, K. Itoh and T. S. Hahm, "Zonal flows in plasma—a review", Plasma Phys. Contr. Fusion **47** (2005) R35-R161.
[61] J. E. Kinsey, R. E. Waltz and J. Candy, "Nonlinear gyrokinetic turbulence simulations of E×B shear quenching of transport", Phys. Plasmas **12** (2005) 062302.
[62] H. L. Kuo, "Perturbations of Plane Couette Flow in Stratified Fluid and Origin of Cloud Streets", Phys. Fluids **6** (1963) 195-211.

[63] B. Lehnert, "Short-Circuit of Flute Disturbances at a Plasma Boundary" Phys. Fluids **9** (1966) 1367-1372.
[64] A. Hassam, "Nonlinear stabilization of the Rayleigh-Taylor instability by external velocity shear", Phys. Plasmas **4** (1992) 485-487.
[65] T. Tatsuno, F. Volponi, and Z. Yoshida, "Transient phenomena and secularity of linear interchange instabilities with shear flows in homogeneous magnetic field plasmas", Phys. Plasmas **8** (2001) 399-406.
[66] Y. Zhang, S. I. Krasheninnikov, and A. I. Smolyakov "Velocity shear effects on localized interchange and resistive drift wave instabilities", Phys. Plasmas **27** (2020) 020701.
[67] E. S. Benilov, V. Naulin, and J. Juul Rasmussen, "Does a sheared flow stabilize inversely stratified fluid?", Physics of Fluids **14** (2002) 1674-1680.
[68] B. A. Carreras, V. E. Lynch, L. Garcia, and P. H. Diamond, "Resistive pressure-gradient-driven turbulence with self-consistent flow profile evolution" Phys. Plasmas **5** (1993) 1491-1505.
[69] H. Sugama and M. Wakatani "Radial electric field effect on resistive interchange modes", Phys. Plasmas **3** (1991) 1110-1112.
[70] M. V. Medvedev and P. H. Diamond, "Theory of ideal magnetohydrodynamic ballooning stability of a poloidally rotating plasma in a sheared electric field", Phys. Plasmas **2** (1995) 727-732.
[71] R. L. Miller, F. L. Waelbroeck, A. B. Hassam, and R. E. Waltz, "Stabilization of ballooning modes with sheared toroidal rotation", Phys. Plasmas **2** (1995) 3676-3684.
[72] A. Sen and J. J. Ramos, "Tokamak equilibria and stability with arbitrary flows", Plasma Phys. Control. Fusion **39** (1997) A323–A332.
[73] L. Villard, A. Bottino, O. Sauter, and J. Vaclavik, "Radial electric fields and global electrostatic microinstabilities in tokamaks and stellarators", Phys. Plasmas **9** (2002) 2684-2691.
[74] A. J. Webster and H. R. Wilson, "Role of Flow Shear in the Ballooning Stability of Tokamak Transport Barriers", Phys. Rev. Lett. **92** (2004) 165004.
[75] P. W. Xi, X. Q. Xu, X. G. Wang, and T. Y. Xia, "Influence of equilibrium shear flow on peeling-ballooning instability and edge localized mode crash", Phys. Plasmas **19** (2012) 092503.
[76] J. G. Chen, X. Q. Xu, C. H. Ma, P. W. Xi, D. F. Kong, and Y. A. Lei, "Impact of E×B shear flow on low-n MHD instabilities", Phys. Plasmas **24** (2017) 050704.
[77] V. I. Dagnelie, J. Citrin, F. Jenko, M. J. Pueschel, T. Görler, D. Told, and H. Doerk, "Growth rates of ITG modes in the presence of flow shear", Phys. Plasmas **26** (2012) 012502.
[78] V. I. Dagnelie, "Dynamics of linear ITG modes with flow shear in ballooning space", Master Thesis, Utrecht University, 2017.
[79] P. J. Schmidt, "Linear stability theory and bypass transition in shear flows", Phys. Plasmas **7** (2000) 1788-1794.
[80] L. Trefethen and M. Embree, "Spectra and Pseudospectra: The Behavior of Nonnormal Matrices and Operators" (Princeton University Press, Princeton, NJ, 2005).
[81] A. B. Hassam, "Nonlinear stabilization of the Rayleigh-Taylor instability by external velocity shear", Phys. Plasmas **4** (1992) 485-487.
[82] V. S. Mikhailenko, V. V. Mikhailenko, J. Weiland, "Rayleigh-Taylor instability in plasma with shear flow", Phys. Plasmas **9** (2002) 2891-2895.

[83] N. Mattor and P. H. Diamond, "Drift wave propagation as a source of plasma edge turbulence: Slab theory", Phys. Plasmas **1** (1994) 4002-4013.
[84] J. Boedo, D. Gray, S. Jachmich, R. Conn, G. P. Terry, G. Tynan, G. Van Oost, R. R. Weynants, TEXTOR Team, "Enhanced particle con_nement and turbulence reduction due to E×B shear in the TEXTOR tokamak", Nucl. Fusion **40** (2000) 1397-1410.
[85] G. Van Oost, J. Adámek, V. Antoni, P. Balan, J. A. Boedo, P. Devynck, I. Ďuran, L. Eliseev, J. P. Gunn, M. Hron, C. Ionita, S. Jachmich, G. S. Kirnev, E. Martines, A. Melnikov, R. Schrittwieser, C. Silva, J. Stöckel, M. Tendler, C. Varandas, M. Van Schoor, V. Vershkov and R. R. Weynants, "Turbulent transport reduction by E×B velocity shear during edge plasma biasing: recent experimental results", Plasma Phys. Contr. Fusion **45** (2003) 621-643.
[86] H. Biglari, P. H. Diamond, and P. W. Terry, "Influence of sheared poloidal rotation on edge turbulence", Phys. Fluids B **2** (1990) 1-4.
[87] K. Itoh and S.-I. Itoh "The role of the electric field in confinement", Plasma Phys. Contr. Fusion **38** (1996) 1-49.
[88] K. H. Burrell, "Effects of E×B velocity shear and magnetic shear on turbulence and transport in magnetic confinement devices", Phys. Plasmas **4** (1997) 1499-1518.
[89] F. Wagner, "A quarter-century of H-mode studies", Plasma Phys. Contr. Fusion **49** (2007) B1-B33.
[90] G. R. Tynan, A. Fujisawa and G. McKee, "A review of experimental drift turbulence studies", Plasma Phys. Contr. Fusion **51** (2009) 113001.
[91] A. Fujisawa, "Experimental studies of mesoscale structure and its interactions with microscale waves in plasma turbulence", Plasma Phys. Contr. Fusion **53** (2011) 124015.
[92] J. W. Connor, G. F. Counsell, S. K. Erents, S. J. Fielding, B. LaBombard, K. Morel, "Comparison of theoretical models for scrape-off layer widths with data from COMPASS-D, JET and Alcator C-Mod", Nucl. Fusion **39** (1999) 169-188.
[93] J. A. Krommes,"A tutorial introduction to the statistical theory of turbulent plasmas, a half-century after Kadomtsev's Plasma Turbulence and the resonance-broadening theory of Dupree and Weinstock", J. Plasma Physics **81** (2015) 205810601.
[94] A. I. Smolyakov, P. H. Diamond, and V. I. Shevchenko, "Zonal flow generation by parametric instability in magnetized plasmas and geostrophic fluids", Phys. Plasmas **7** (2000) 1349-1351.
[95] P. H. Diamond, M. N. Rosenbluth, F. L. Hinton, M. Malkov, J. Fleischer, and A. Smolyakov, 17th IAEA Fusion Energy Conference, IAEA-CN-69/TH3/1 (International Atomic Energy Agency, Vienna, 1998).
[96] J. P. Terry, private communication, 2018.
[97] R. J. Maqueda, G. A. Wurden, D. P. Stotler, S. J. Zweben, B. LaBombard, J. L. Terry, J. L. Lowrance, V. J. Mastrocola, G. F. Renda, D. A. D'Ippolito, J. R. Myra, N. Nishino, "Gas puff imaging of edge turbulence", Rev. Scientific Instruments **74** (2003) 2020-2026.
[98] S. I. Krasheninnikov, D. A. D'Ippolito, and J. R. Myra," Recent theoretical progress in understanding coherent structures in edge and SOL turbulence", J. Plasma Physics **74** (2008) 679-717.
[99] S. I. Krasheninnikov, A. Yu. Pigarov, T. K. Soboleva, and D. L. Rudakov, "Strongly intermittent edge plasma transport: Issues with modeling and interpretation of experimental data", Phys. Plasmas **16** (2008) 014501.
[100] D. A. D'Ippolito, J. R. Myra, and S. J. Zweben, "Convective transport by intermittent blob-filaments: Comparison of theory and experiment", Phys. Plasmas **18** (2011) 060501.

[101] S. I. Krasheninnikov, "Physical mechanisms in divertors and their impact on the core", Czech. J. Phys. **48** (1998) 97-112.
[102] S. I. Krasheninnikov, "On scrape off layer plasma transport", Phys. Lett. A **283** (2001) 368-370.
[103] M. Greenwald, D. Andelin, N. Basse, S. Bernabei, P. Bonoli, B. Böse, C. Boswell, R. Bravenec, B. Carreras, I. Cziegler, E. Edlund, D. Ernst, C. Fasoli, M. Ferrara, C. Fiore, R. Granetz, O. Grulke, T. Hender, J. Hosea, D.H. Howell, A. Hubbard, J. Hughes, I. Hutchinso1, A. Ince-Cushman, J. Irby, B. LaBombard, R. LaHaye, L. Lin, Y. Lin, B. Lipschultz, J. Liptac, S. Lisgo, A. Lynn, E. Marmar, K. Marr, D. R. Mikkelsen, R. McDermott, D. Mossessian, A. Parisot, R. Parker, C. Phillips, P. Phillips, M. Porkolab, M. Redi, J. Rice, W. Rowan, M. Sampsell, G. Schilling, S. Scott, J. T. Scoville, N. Smick, J. Snipes, P. Stangeby, V. Tang, J. Terry, M. Ulrickson, G. Wallace, D. Whyte, J.Wilson, J.Wright, S. Wolfe, S. Wukitch, B. Youngblood, H. Yuh, K. Zhurovich and S. Zweben,"Overview of the Alcator C-Mod program", Nucl. Fusion **45** (2005) S109
[104] H. J. Sun, E. Wolfrum, T. Eich, B. Kurzan, S. Potzel, U. Stroth, and the ASDEX Upgrade Team, "Study of near scrape-off layer (SOL) temperature and density gradient lengths with Thomson scattering", Plasma Phys. Contr. Fusion **57** (2015) 125011.
[105] N. Bisai, R. Jha, and P. K. Kaw, "Role of neutral gas in scrape-off layer tokamak plasma", Phys. Plasmas **22** (2015) 022517.
[106] D. P. Stotler, J. Lang, C. S. Chang, R. M. Churchill and S. Ku, "Neutral recycling effects on ITG turbulence", Nucl. Fusion **57** (2017) 086028.
[107] B. D. Dudson, M. V. Umansky, X. Q. Xu, P. B. Snyder, H. R. Wilson, "BOUT++: a framework for parallel plasma fluid simulations", Comp. Phys. Comm., **180** (2009) 1467-1480.
[108] C. S. Chang, S. Ku, A. Loarte, V. Parail, F. Köchl, M. Romanelli, R. Maingi, J.-W. Ahn, T. Gray, J. Hughes, B. LaBombard, T. Leonard, M. Makowski and J. Terry, "Gyrokinetic projection of the divertor heat-flux width from present tokamaks to ITER", Nucl. Fusion **57** (2017) 116023.
[109] D. Told, F. Jenko , J.M. TenBarge, G.G. Howes, G.W. Hammett, "Multiscale nature of the dissipation range in gyrokinetic simulations of Alfvénic turbulence", Phys. Rev. Lett. **115** (2015) 025003.
[110] T. N. Bernard, E. L. Shi, K. W. Gentle, A. Hakim, G. W. Hammett, T. Stoltzfus-Dueck, and E. I. Taylor, "Gyrokinetic continuum simulations of plasma turbulence in the Texas Helimak", Phys. Plasmas **26** (2019) 042301.
[111] F. J. Artola, G. T. A. Huijsmans, M. Hoelzl, P. Beyer, A. Loarte, Gribov Y. "Non-linear magnetohydrodynamic simulations of Edge Localised Modes triggering via vertical oscillations" Nucl. Fusion, **58** (2018) 096018.
[112] A. E. Gill, "Atmosphere-Ocean Dynamics" (Academic Press, New York, 1982).
[113] R. Fjørtoft, "On the changes in the spectral distribution of kinetic energy for twodimensional, nondivergent flow", Tellus **5** (1953) 225.
[114] R. H. Kraichnan, "Inertial Ranges in Two-Dimensional Turbulence" Phys. Fluids **10** (1967) 1417-1423.
[115] A. Hasegawa and K. Mima, "Pseudo-three-dimensional turbulence in magnetized nonuniform plasma", Phys. Fluids **21** (1978) 87-92.
[116] J. G. Charney, "On the scale of atmospheric motions", Geophys. Public **17** (1948) 3-17.
[117] R. Z. Sagdeev, V. D. Shapiro, and V. I. Shevchenko, "Convective cells and anomalous

plasma diffusion", Sov. J. Plasma Phys. **4** (1978) 306-310.
[118] G. Manfredi, C. M. Roach and R. O. Dendy "Zonal flow and streamer generation in drift turbulence", Plasma Phys. Contr. Fusion **43** (2001) 825-937.
[119] R. L. Dewar and R. F. Abdullatif "Zonal flow generation by modultional instability", World Scientific Lecture Notes in Complex Systems, Frontiers in Turbulence and Coherent Structures, (2007) 415-430.
[120] A. M. Balk, "Angular distribution of Rossby wave energy", Phys. Lett. A **345** (2005) 154-160.
[121] C. Connaughton, S. Nazarenko, B. Quinn, "Rossby and drift wave turbulence and zonal flows: the Charney-Hasegawa-Mima model and its extantion", Phys. Reports **604** (2015) 1-71.
[122] L. Villard, P. Angelino, A. Bottino, S. Brunner, S. Jolliet, B. F. McMillan, T. M. Tran and T. Vernay , "Global gyrokinetic ion temperature gradient turbulence simulations of ITER", Plasma Phys. Contr. Fusion **55** (2013) 074017.
[123] T. Lan, A. D. Liu, C. X. Yu, L. W. Yan, W. Y. Hong, K. J. Zhao, J. Q. Dong, J. Qian, J. Cheng, D. L. Yu and Q. W. Yang, "Spectral characteristics of geodesic acoustic mode in the HL-2A tokamak", Plasma Phys. Contr. Fusion **50** (2008) 045002.
[124] L. Vermare, P. Hennequin, Ö. D. Göurcan, X. Garbet, C. Honoré, F. Clairet, J. C. Giacalone, P. Morel, A. Storelli, and Tore Supra Team, "Poloidal asymmetries of flows in the Tore Supra tokamak", Phys. Plasmas **25** (2018) 020704.
[125] S. J. Zweben, "Search for coherent structure within tokamak plasma turbulence", Phys. Fluids **28** (1985) 974-982.
[126] J. A. Boedo, D. Rudakov, R. Moyer, S. Krasheninnikov, D. Whyte, G. McKee, G. Tynan, M. Schaffer, P. Stangeby, P. West, S. Allen, T. Evans, R. Fonck, E. Hollmann, A. M. A. Leonard, G. Porter, M. Tillack, and G. Antar, "Transport by intermittent convection in the boundary of the DIII-D tokamak" Phys. Plasmas **8** (2001) 4826.
[127] M. V. Umansky, S. I. Krasheninnikov, B. LaBombard, J. L. Terry, "Comments on particle and energy balance in the edge plasma of Alcator C-Mod", Phys. Plasmas **5** (1998) 3373-3376.
[128] S. J. Zweben, J. A. Boedo, O. Grulke, C. Hidalgo, B. LaBombard, R. J. Maqueda, P. Scarin and J. L. Terry "Edge turbulence measurements in toroidal fusion devices", Plasma Phys. Contr. Fusion **49** (2007) S1-S23.
[129] G. Fuchert, G. Birkenmeier, B. Nold, M. Ramisch and U. Stroth, "The influence of plasma edge dynamics on blob properties in the stellarator TJ-K",Plasma Phys. Contr. Fusion **55** (2013) 125002.
[130] H. Tanaka, S. Masuzaki, N. Ohno, T. Morisaki, Y. Tsuji, LHD Experiment Group, "Multi-pin Langmuir probe measurement for identification of blob propagation characteristics in the Large Helical Device", J. Nucl. Mater. **463** (2015) 761-764.
[131] B. Ph. van Milligen, J. H. Nicolau, B. Liu, G. Grenfell, U. Losada, B. A. Carreras, L. García, C. Hidalgo and The TJ-II Team, "Filaments in the edge confinement region of TJ-II", Nucl. Fusion **58** (2018) 026030.
[132] J. R. Angus and S. I. Krasheninnikov, "Inciscid evolution of large amplitude filaments in a uniform gravity field", Phys. Plasmas **21** (2014) 112504.
[133] D. L. Rudakov, J. A. Boedo, R. A. Moyer, P. C. Stangeby, J. G.Watkins, D. G. Whyte, L. Zeng, N. H. Brooks, R. P. Doerner, T. E. Evans, M. E. Fenstermacher, M. Groth, E. M. Hollmann, S. I. Krasheninnikov, C. J. Lasnier, A. W. Leonard, M. A. Mahdavi, G. R. McKee, A. G. McLean, A. Yu. Pigarov, W. R.Wampler, G. Wang, W. P. West and C. P. C.Wong, "Far

SOL transport and main wall plasma interaction in DIII-D", Nucl. Fusion **45** (2005) 1589-1599.

[134] C. Theiler, I. Furno, P. Ricci, A. Fasoli, B. Labit, S. H. Műller, and G. Plyushchev, "Cross-Field Motion of Plasma Blobs in an Open Magnetic Field Line Configuration" Phys. Rev. Lett. **103** (2009) 065001.

[135] B. Lloyd, R. J. Akers, F. Alladio, Y. Andrew, L. C. Appel, D. Applegate, K. B. Axon, N. Ben Ayed, C. Bunting, R. J. Buttery, P. G. Carolan, I. Chapman, D. Ciric, J. W. Connor, N. J. Conway, M. Cox, G. F. Counsell, G. Cunningham, A. Darke, E. Delchambre, R. O. Dendy, J. Dowling, B. Dudson, M. Dunstan, A. R. Field, A. Foster, S. Gee, L. Garzotti, M. P. Gryaznevich, A. Gurchenko, E. Gusakov, N. C. Hawkes, P. Helander, T. C. Hender, B. Hnat, D. F. Howell, N. Joiner, D. Keeling, A. Kirk, B. Koch, M. Kuldkepp, S. Lisgo, F. Lott, G. P. Maddison, R. Maingi, A. Mancuso, S. J. Manhood, R. Martin, G. J. McArdle, J. McCone, H. Meyer, P. Micozzi, A. W. Morris, D. G. Muir, M. Nelson, M. R. O'Brien, A. Patel, S. Pinches, J. Preinhaelter, M. N. Price, E. Rachlew, C. M. Roach, V. Rozhansky, S. Saarelma, A. Saveliev, R. Scannell, S. E. Sharapov, V. Shevchenko, S. Shibaev, K. Stammers, J. Storrs, A. Surkov, A. Sykes, S. Tallents, D. Taylor, N. Thomas-Davies, M. R. Turnyanskiy, J. Urban, M. Valovic, R. G. L. Vann, F. Volpe, G. Voss, M. J. Walsh, S. E. V.Warder, R. Watkins, H. R. Wilson, M. Wisse and the MAST and NBI teams, "Overview of physics results from MAST" ", Nucl. Fusion **47** (2007) S658-S667.

[136] A. Kirk, N. Ben Ayed, G. Counsell, B. Dudson, T. Eich, A. Herrmann, B. Koch, R. Martin, A. Meakins, S. Saarelma, R. Scannell, S. Tallents, M. Walsh, H. R. Wilson and the MAST team, "Filament structures at the plasma edge on MAST", Plasma Phys. Contr. Fusion **48** (2006) B433-B441.

[137] R. J. Maqueda, D. P. Stotler, S. J. Zweben, The NSTX team, "Intermittency in the scape-off layer of the National Spherical Torus Experiment during H-mode confinement", J. Nucl. Materials **415** (2011) S459-S462.

[138] G. Q. Yu and S. I. Krasheninnikov, "Dynamics of blobs in scrape-off-layer/shadow regions of tokamaks and linear devices", Phys. Plasmas **10** (2003) 4413-4418.

[139] J. Angus, M. Umansky, and S. Krasheninnikov, "Effect of Drift Waves on Blob Dynamics", Phys. Rev. Letters **108** (2012) 215002.

[140] N. Vianello, C. Tsui, C. Theiler, S. Allan, J. Boedo, B. Labit, H. Reimerdes, K. Verhaegh, W.A.J. Vijvers, N. Walkden, S. Costea, J. Kovacic, C. Ionita, V. Naulin, A.H. Nielsen, J. Juul Rasmussen, B. Schneider, R. Schrittwieser, M. Spolaore, D. Carralero, J. Madsen, B. Lipschultz, F. Militello, The TCV Team and The EUROfusion MST1Team, "Modification of SOL profiles and fluctuations with line-average density and divertor flux expansion in TCV", Nucl. Fusion **57** (2017) 116014.

[141] E. L. Shi, G. W. Hammett, T. Stoltzfus-Dueck, and A. Hakim, "Full-f gyrokinetic simulation of turbulence in a helical open-field-line plasma", Phys. Plasmas **26** (2019) 012307.

[142] S. I. Krasheninnikov, "On the origin of plasma density blobs", Phys. Lett. A **380** (2016) 3905-3907.

[143] D. Galassi, P. Tamain, H. Bufferand, G. Ciraolo, Ph. Ghendrih, C. Baudoin, C. Colin, N. Fedorczak, N. Nace and E. Serre, "Drive of parallel flows by turbulence and large-scale E×B transverse transport in divertor geometry" Nucl. Fusion **57** (2017) 036029.

[144] P. Paruta, P. Ricci, F. Riva, C. Wersal, C. Beadle, and B. Frei, "Simulation of plasma turbulence in the periphery of diverted tokamak by using the GBS code", Phys. Plasmas **25** (2018) 112301.

[145] A. Stegmeir, A. Ross, T. Body, M. Francisquez, W. Zholobenko, D. Coster, O. Maj, P.

Manz, F. Jenko, B. N. Rogers, and K. S. Kang, “Global turbulence simulations of the tokamak edge region with GRILLIX”, Phys. Plasmas **26** (2019) 052517.
[146] T. Eich, A. W. Leonard, R. A. Pitts, W. Fundamenski, R. J. Goldston, T. K. Gray, A. Herrmann, A. Kirk, A. Kallenbach, O. Kardaun, A. S. Kukushkin, B. LaBombard, R. Maingi, M.A. Makowski, A. Scarabosio, B. Sieglin, J. Terry, A. Thornton and ASDEX Upgrade Team and JET EFDA Contributors, “Scaling of the tokamak near the scrape-off layer H-mode power width and implications for ITER” Nucl. Fusion **53** (2013) 093031.
[147] R. J. Goldston “Heuristic drift-based model of the power scrape-off width in low-gas-puff H-mode tokamaks” Nucl. Fusion **52** (2012) 013009.
[148] X. Q. Xu, N. M. Li, Z.Y. Li, B. Chen, T. Y. Xia, T. F. Tang, G. Z. Deng, B. Zhu, and V. S. Chan, “Simulations of tokamak boundary plasma turbulent transport in setting the divertor heat flux width”, 27th IAEA Fusion Energy Conference, IAEA-CN-123/45/TH/P7-21.
[149] Ze-Yu Li, X. Q. Xu, Na-Mi Li, V. S. Chan and Xiao-Gang Wang, “Prediction of divertor heat flux width for ITER using BOUT++ transport and turbulence module”, Nucl. Fusion **59** (2019) 046014.